CoMP Transmission in Downlink NOMA-Based Cellular-Connected UAV Networks

Hongguang Sun, *Member, IEEE,* Linyi Zhang, Tony Q. S. Quek, *Fellow, IEEE,* Xijun Wang, *Member, IEEE,* and Yan Zhang, *Member, IEEE*

Abstract

In this paper, we study the integration between the coordinated multipoint (CoMP) transmission and the non-orthogonal multiple access (NOMA) in the downlink cellular-connected UAV networks with the coexistence of aerial users (AUs) and terrestrial users (TUs). Based on the comparison of the desired signal strength to the dominant interference strength, the AUs are classified into CoMP-AUs and Non-CoMP AUs, where the former receives transmissions from two cooperative BSs, and constructs two exclusive NOMA clusters with two TUs, respectively. A Non-CoMP AU constructs a NOMA cluster with a TU served by the same BS. By leveraging the tools from stochastic geometry, we propose a novel analytical framework to evaluate the performance of the CoMP-NOMA based cellular-connected UAV network in terms of coverage probability, and average ergodic rate. We reveal the superiority of the proposed CoMP-NOMA scheme by comparing with three benchmark schemes, and further quantify the impacts of key system parameters on the network performance. By harvesting the benefits of both CoMP and NOMA, we prove that the proposed framework can provide reliable connection for AUs by using CoMP and enhance the average ergodic rate through NOMA technique as well.

Index Terms

Cellular-connected UAV networks, CoMP, NOMA, Stochastic Geometry.

Hongguang Sun, and Linyi Zhang are with the College of Information Engineering, Northwest A&F University, Yangling 712100, China (e-mail: hgsun@nwafu.edu.cn; LinyiZhang2020@163.com;).

Tony Q. S. Quek is with the Information Systems Technology and Design Pillar, Singapore University of Technology and Design, Singapore 487372 (e-mail: tonyquek@sutd.edu.sg).

Xijun Wang is with the School of Electronics and Information Technology, Sun Yat-sen University, Guangzhou 510006, China (email: wangxijun@mail.sysu.edu.cn).

Yan Zhang is with the State Key Laboratory of Integrated Service Networks, Xidian University, Xi'an 710071, China (e-mail: yanzhang@xidian.edu.cn).

I. INTRODUCTION

Recently, unmanned aerial vehicle (UAV) has found its various applications in a wide range of areas, such as agriculture, disaster rescue and other civil industries. To support the realization of UAV communications, it's essential to maintain a reliable connection between the UAV and the operator [1]–[3]. Thanks to the pervasive deployment of cellular networks, cellular-connected UAV has been served as a new paradigm to provide ubiquitous connectivity for the newly joined aerial users (AUs) as well as the existing terrestrial users (TUs) [4]–[7].

Unfortunately, there still exists major challenges for achieving satisfactory service quality for AUs. On one hand, existing cellular architectures are primarily designed for TUs, where base stations (BSs) are equipped with down-tilted antennas to improve the desired signal strength and decrease the inter-cell interference (ICI) of TUs. As a result, the high-altitude AUs can only be served by the BS's sidelobe, leading to the poor coverage probability and achievable rate. On the other hand, the integration of AUs into the existing cellular networks also leads to the performance degradation of coexisting TUs due to the spectrum sharing and the resulted extra interference [8]. Therefore, it is of great significance to design advanced technologies to enable the harmonious coexistence between AUs and TUs. The authors in [9] [10] studied the opposite effects of line-of-sight (LoS) transmissions on the incremental received signal power and the extra aggregated interference, which shows that the adversities dominate the benefits. The spectrum sharing between UAV-to-UAV transmissions and uplink cellular transmissions was investigated in [11] where the performance for both underlay mode and overlay mode was analyzed. A comprehensive performance analysis framework for the downlink cellular-connected UAV network was proposed in [12], in which the impacts of tilting the UAV antenna, the traffic load, and the network densification on the coverage probability or achievable throughput were evaluated. The directional antennas were equipped by AUs in [13] to restrict the number of interfering downlink BSs.

Coordinated multipoint (CoMP) transmission technique has been considered as an effective approach to diminish the negative effect of LoS interference. The authors in [14] designed the CoMP transmission scheme for UAV BSs to forward signals from TUs to a central processor. The work in [15] exploited downlink coherent CoMP transmissions to support static and three-dimensional (3D) mobile AUs, and verified the effect of CoMP in improving the coverage probability. Although CoMP transmissions can boost the network performance, it results in the

waste of channel resources, limits the number of users that can be simultaneously served, and deteriorates the spectral efficiency [16] [17]. For CoMP transmissions in downlink, all associated BSs for CoMP need to allocate the same channel to a cell-edge user and this channel cannot be allocated to other users simultaneously when orthogonal multiple access (OMA) techniques are employed. The network performance is getting even worse with the increasing number of cell-edge users [16].

In order to enhance the spectral efficiency, non-orthogonal multiple access (NOMA) has been considered as a promising multiple access technology for the fifth generation (5G) and beyond 5G (B5G) cellular systems [18] [19]. Specifically, to maximize the sum-rate for downlink transmission with the power domain NOMA (PD-NOMA), BS power allocation enables PD-NOMA users to perform the successive interference cancellation (SIC) according to the ascending order of their channel gains [20]. System-level and link-level simulations in [21] indicated clear benefits of NOMA over OMA in terms of overall system throughput as well as individual users' throughput. Although the applications of NOMA has been considered in the uplink cellular-connected UAV networks [22]–[25], only few works considered downlink NOMA in such a network scenario. Amongest, the work [26] analyzed the outage probability of AU and TU under the downlink NOMA in a single cell network by leveraging the instantaneous channel gain ranking. A robust NOMA scheme has been proposed in [27] where the TU and AU are paired for the data link and control link, respectively. The work in [28] considered the scenario of two co-channel cells and proposed a cooperative NOMA scheme. However, the impacts of aggregated interference and key system parameters on the performance of NOMA-enabled cellular-connected UAV network have not been investigated. Motivated by this, the work in [29] leveraged the tools from stochastic geometry and proposed an analytical framework to evaluate the network performance under downlink NOMA for coexisting AUs and TUs. However, the utilization of NOMA scheme introduces extra inter-NOMA user interference besides the co-channel interference, which may deteriorate the received Signal-to-Interference-plus-Noise-Ratio (SINR) at AUs which are usually served as far users in NOMA clusters.

To mitigate the severe effect of ICI, improve the whole system spectral efficiency, and satisfy the rate requirements for AUs while reducing deterioration to the TU's performance, the combination of CoMP with NOMA can be served as one of the promising access techniques [30].

In this work, we consider PD-NOMA which is simply referred to as NOMA in the following statements.

Recently, the integration of joint transmission CoMP (JT-CoMP) has been widely discussed in NOMA-based multicell downlink transmissions. To be specific, the work in [31] proposed a joint CoMP C-NOMA for the enhanced cellular system performance, where only TUs were considered by using the Rayleigh channel model. The work in [32] studied a power allocation problem for maximizing the energy efficiency in downlink CoMP systems with NOMA. The work in [33] proposed propose a user grouping and pairing scheme for a CoMP-NOMA-based system. An analytical framework was designed in [34] to evaluate the performance of the proposed CoMP-NOMA scheme in the downlink heterogeneous cloud radio access network (H-CRAN) where the average achievable data rate for each NOMA user was derived by adopting the Rayleigh fading channel model. To the best of our knowledge, the integration of CoMP and NOMA has not been investigated in the cellular-connected UAV networks. Different from the ground-to-ground (G2G) transmissions in the traditional terrestrial cellular networks, the air-to-ground (A2G) channels exhibit a rather different behavior experiencing the LoS transmissions which is dependent on the altitude of AUs. As such, the existing CoMP-NOMA schemes cannot be directly applied to the network scenarios incorporating AUs and TUs. Specifically, the CoMP-NOMA scheme should be carefully designed to exploit the asymmetric channel fading for A2G link and G2G link, and an analytical framework should be developed to thoroughly characterize the gain achieved by the CoMP-NOMA scheme in the cellular-connected UAV networks.

Motivated by the aforementioned, in this paper, we study the amalgamation between JT-CoMP and NOMA technologies in the downlink cellular-connected UAV networks to enhance the spectral efficiency of the whole network, and provide a reliable connection for AUs as well. To the best of our knowledge, the application of a joint interference-aware JT-CoMP with NOMA scheme to the cellular-connected UAV network using tools from stochastic geometry has not been investigated. Our main contributions are listed as follows:

- We investigate the joint efforts of interference-aware JT-CoMP and NOMA in enhancing the performance for downlink transmissions of a cellular-connected UAV network, where AUs that are vulnerable to ICI are prioritized to trigger the JT-CoMP. Specifically, the AUs are divided into two categories, namely, CoMP-AUs and Non-CoMP AUs. A CoMP AU is allowed to receive transmissions from two cooperative BSs, and constructs two exclusive NOMA clusters with two TUs which are served by the two corresponding BSs, respectively. A Non-CoMP AU is served by one BS and constructs a NOMA cluster with a TU served

by the same BS.

- By leveraging the tools from stochastic geometry, we propose a novel analytical framework to evaluate the performance of the CoMP-NOMA based cellular-connected UAV network in terms of coverage probability for AUs and TUs, the average achievable rate for each user in each NOMA cluster, and the spectral efficiency of the network. Due to the existence of LoS and NLoS A2G transmissions, the expression of the corresponding SIR at the CoMP-AU is different from that of either the existing CoMP-OMA and NOMA-Only schemes for cellular-connected UAVs, nor the traditional CoMP-NOMA scheme for the traditional TUs. By using the Cauchy-Schwarz's inequality and Gamma approximations, we derive the computationally tractable expressions for the above performance metrics.

- We validate the theoretical analysis by using Monte Carlo simulations, and show the superiority of the proposed CoMP-NOMA scheme by comparing with the NOMA-Only, CoMP-OMA and OMA-Only schemes. We further evaluate the impacts on network performance of key system parameters, such as SIR threshold, BS density, AU's altitude, cooperation threshold, and power allocation coefficient allocated to AU and TU within a NOMA cluster. We then provide practical guidelines for an efficient design of the proposed CoMP-NOMA scheme by optimizing the cooperation threshold, AU's altitude and power control coefficients for AU and TU within a NOMA pair.

The rest of the paper is organized as follows: Section II details the system model, and the proposed COMP-NOMA framework. Section III derives the relevant distance distributions and the association probabilities. Section IV presents the performance analysis in terms of coverage probability and average ergodic rate. The simulation and analytical results are then provided in Section V, followed by the conclusions drawn in Section VI.

II. SYSTEM MODEL

A. Network Model

In this paper, we consider a downlink cellular-connected UAV network where BSs are distributed according to a homogeneous PPP Φ_B of intensity λ_b with a fixed height h_b. The spatial locations of TUs and AUs follow two other homogeneous PPPs of intensities λ_t and λ_u with fixed heights h_t and h_u, respectively. We assume a fully-loaded network scenario, i.e., $\lambda_t \gg \lambda_b$, and $\lambda_u \gg \lambda_b$, such that each BS has at least one TU and one AU to associate with. We consider the random scheduling scheme, and a BS randomly selects an AU and a TU to serve

if more than one AU and/or TU are associated with the BS. The BS antenna is assumed to have vertically directional and horizontally omnidirectional radiation pattern, which can be realized by implementing multiple sector antennas. In practice, the BS antennas are usually down-tilted to provide better coverage for TUs. As such, TUs are assumed to be served by BSs via mainlobe with antenna gain g_{M}, and AUs above BSs height are assumed to be served by BSs via sidelobe with antenna gain g_{m} [12]. Without loss of generality, we focus on the performance of a typical pair of AU and TU. By Slivynak's theorem, the typical AU is assumed to be located at the origin with a fixed altitude of h_{u}. In addition, we define $\Delta h_{\mathrm{u}} \triangleq |h_{\mathrm{u}} - h_{\mathrm{b}}|$ as the height difference between a BS and a random AU, and $\Delta h_{\mathrm{t}} \triangleq |h_{\mathrm{t}} - h_{\mathrm{b}}|$ as the height difference between a BS and a random TU.

B. Channel Model

The channel model consists of large-scale path loss and small-scale fading. For the aerial communication link between the typical AU and the BS, we consider a practical path loss model incorporating both LoS and NLoS transmissions, where a probabilistic function is employed to compute the LoS probability [35]:

$$p^{\mathrm{L}}(z) = \frac{1}{1 + C \exp\left(-B\left[\frac{180}{\pi}\arctan(\Delta h_{\mathrm{u}}/z) - C\right]\right)}, \tag{1}$$

where z is the Euclidean horizontal distance between the typical AU and the considered BS, C and B are environment-dependent constants, $\arctan(\Delta h_{\mathrm{u}}/z)$ is the elevation angle between an AU and a BS. The NLoS probability between an AU and a BS given by $p^{\mathrm{N}}(z) = 1 - p^{\mathrm{L}}(z)$. Note that $z = \sqrt{r^2 - (\Delta h_{\mathrm{u}})^2}$, where r is the 3D distance between the AU and the BS. Thus, the LoS probability can also be expressed as a function of r, i.e., $p^{\mathrm{L}}(r) = p^{\mathrm{L}}(z)|_{z=\sqrt{r^2-(\Delta h_{\mathrm{u}})^2}}$. Based on the A2G channel model in (1), we assume that each AU experiences either LoS or NLoS transmission with a BS independently. From the typical AU's perspective, the set of BSs Φ_{B} can be decomposed into two inhomogeneous PPPs, i.e., $\Phi_{\mathrm{B}}^{\mathrm{L}}$ and $\Phi_{\mathrm{B}}^{\mathrm{N}}$, of intensities $\lambda_{\mathrm{B}} p^{\mathrm{L}}(z)$ and $\lambda_{\mathrm{B}}(1 - p^{\mathrm{L}}(z))$, respectively. For the sake of clarity, we define a BS as a LoS (NLoS) BS, if the typical AU experiences the LoS (NLoS) transmission to the BS.

The large-scale path loss between the typical AU and its associated BS b_0 is expressed as

$$\zeta_v(b_0) = A_v g_{\mathrm{m}} r_{\mathrm{b}_v,\mathrm{u}}^{-\alpha_v}, v \in \{\mathrm{L}, \mathrm{N}\}, \tag{2}$$
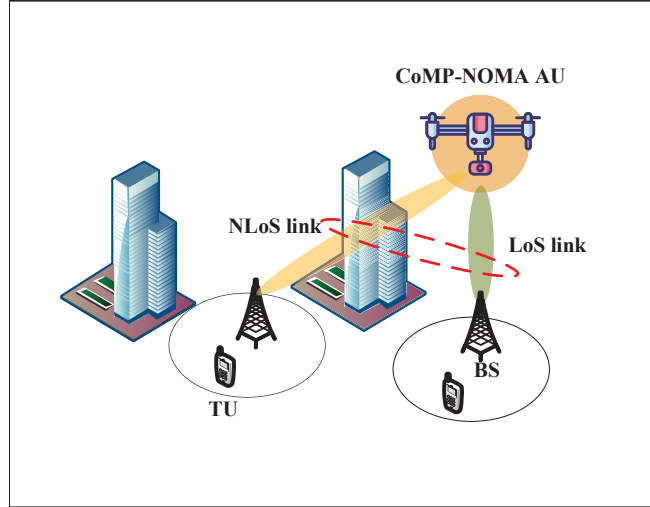
Fig. 1. An illustration of the proposed CoMP-NOMA scheme for cellular-connected UAV network.

where v denotes the type of A2G links with L and N being short for LoS and NLoS, respectively. The symbol A_v denotes the path loss constant at the reference distance $d_i = 1m$ for the type v link, α_v is defined as the path loss exponent for the type v link, and g_{m} is the antenna sidelobe gain provided by its associated BS. For simplicity, we define $\eta_v \triangleq A_v g_{\mathrm{m}}$, $v \in \{\mathrm{L}, \mathrm{N}\}$.

For small-scale fading, we adopt the Nakagami-m model with the probability distribution function (PDF) given by $f(\omega) = \dfrac{2m_v^{m_v} \omega^{2m_v-1}}{\Gamma(m_v)} \exp(-m_v \omega^2)$, where m_v, $v \in\{\mathrm{L},\ \mathrm{N}\}$ is the fading parameter assumed to be an integer for analytical tractability with $m_{\mathrm{L}} > m_{\mathrm{N}}$. Given $\omega \sim \mathrm{Nakagami}(m_v)$, it directly follows that the channel power gain $|\omega|^2 \sim \mathrm{Gamma}(m_v, 1/m_v)$, where $\mathrm{Gamma}(K, \Theta)$ is the Gamma distribution with K and Θ denoting the shape parameter and scale parameter, respectively.

The large-scale path loss between the typical TU and the tagged BS is

$$\zeta_{\mathrm{t}}(b) = A_{\mathrm{t}} g_{\mathrm{M}} r_{\mathrm{b,t}}^{-\alpha_{\mathrm{t}}}, \tag{3}$$

where A_{t} is the attenuation for the terrestrial link, g_{M} is the antenna mainlobe gain provided by its associated BS, and α_t denotes the terrestrial path loss exponent. For simplicity, we define $\eta_{\mathrm{t}} \triangleq A_{\mathrm{t}} g_{\mathrm{M}}$. The small-scale fading between a TU and a BS is exponentially distributed with the unit mean, which corresponds to the Rayleigh fading.

C. User Association and Classification of AUs

In this paper, we consider the strongest average received signal strength (RSS) association policy for both AUs and TUs. For a TU, the strongest average RSS association policy is equivalent to the nearest association policy. Therefore, the PDF of the distance between the typical TU and its serving BS is given by $f_R(r) = 2\pi\lambda_b r \exp(-\pi\lambda_b(r^2 - \Delta h_t^2))$, $r \geq \Delta h_t$ [36]. For an AU, due to the LoS/NLoS transmissions, the nearest BS may not be the one providing the strongest average RSS. What's more, we consider the cooperative transmissions for eligible AUs which is served by two BSs. The AUs are classified into Non-CoMP AUs, and CoMP AUs. A CoMP AU is served by the two BSs that provide the first two strongest average RSS, and constructs two exclusive NOMA clusters with two corresponding TUs served by each of the two BSs as shown in Fig. 1. As a result, each CoMP AU is treated as a member in the two corresponding NOMA clusters. For a Non-CoMP AU, it is served by the BS that provides the strongest average RSS, and as a member of a single NOMA cluster. According to the user association policy, the serving BS(s) of a Non-CoMP AU and a CoMP AU are, respectively, selected as follows

$$b_0 = \{b_0 \mid \max \zeta_v(b_v), \forall b_v \in \Phi_B, v \in \{L, N\}\}, \tag{4}$$

$$\{b_0, b_1\} = \{(b_0, b_1) \mid \max\{(\zeta_u(b_u), \zeta_v(b_v))\}, \forall(b_u, b_v) \in \Phi_B, u, v \in \{L, N\}\}. \tag{5}$$

Similarly, the serving BS of a TU is selected as follows

$$b_0 = \{b_0 \mid \max \zeta_t(b), \forall b \in \Phi_B\}. \tag{6}$$

We consider an interference-aware AU classification criteria, which is designed based on the ratio of the received signal power from the serving BS, i.e., the BS providing the strongest average RSS, to that from the dominant interfering BS, i.e., the BS providing the second strongest average RSS. Specifically, we define $\theta > 1$ as the cooperation threshold. If the aforementioned ratio calculated by an AU is smaller than θ, the cooperation is activated, and the AU is referred to as the CoMP AU. Otherwise, the AU is only served by the BS providing the strongest average RSS, referred to as the Non-CoMP AU.

For the typical AU, let b_{L_0} and b_{N_0} be its nearest LoS BS and NLoS BS, respectively. It is worth noting that the BS providing the strongest average RSS must be either b_{L_0} or b_{N_0}. Similarly, let b_{L_1} and b_{N_1} be the second nearest LoS BS and NLoS BS of the typical AU, respectively. Define

TABLE I
CLASSIFICATION OF AUs

Type of AUs	Condition	Type of BSs	Serving BS Set $\mathcal{B}$
Non-CoMP	$\dfrac{\zeta_{\mathrm{L}}}{\zeta_{\mathrm{In}}} \geq \theta$	LoS	$\{b_{\mathrm{L}_0}\}$
	$\dfrac{\zeta_{\mathrm{N}}}{\zeta_{\mathrm{In}}} \geq \theta$	NLoS	$\{b_{\mathrm{N}_0}\}$
CoMP	$\dfrac{\zeta_{\mathrm{L}_0}}{\zeta_{\mathrm{L}_1}} < \theta, \dfrac{\zeta_{\mathrm{L}_1}}{\zeta_{\mathrm{N}_0}} > 1$	LoS, LoS	$\{b_{\mathrm{L}_0}, b_{\mathrm{L}_1}\}$
	$\dfrac{\zeta_{\mathrm{N}_0}}{\zeta_{\mathrm{N}_1}} < \theta, \dfrac{\zeta_{\mathrm{N}_1}}{\zeta_{\mathrm{L}_0}} > 1$	NLoS, NLoS	$\{b_{\mathrm{N}_0}, b_{\mathrm{N}_1}\}$
	$\dfrac{\zeta_{\mathrm{L}_0}}{\zeta_{\mathrm{N}_0}} < \theta, \dfrac{\zeta_{\mathrm{N}_0}}{\zeta_{\mathrm{L}_1}} > 1$	LoS, NLoS	$\{b_{\mathrm{L}_0}, b_{\mathrm{N}_0}\}$
	$\dfrac{\zeta_{\mathrm{N}_0}}{\zeta_{\mathrm{L}_0}} < \theta, \dfrac{\zeta_{\mathrm{L}_0}}{\zeta_{\mathrm{N}_1}} > 1$	LoS, LoS	$\{b_{\mathrm{N}_0}, b_{\mathrm{L}_0}\}$

$\mathcal{B}$ as the serving BS set of the typical AU. Based on the aforementioned criteria of AUs , the serving BS set $\mathcal{B}$ has two possibilities for a Non-CoMP AU, and four possibilities for a CoMP AU. To be specific, if the typical AU is a Non-CoMP AU, $\mathcal{B} = \{b_{\mathrm{L}_0}\}$ or $\{b_{\mathrm{N}_0}\}$ depending on the relation between the RSSs from b_{L_0} and b_{N_0}. If the typical AU is a CoMP AU, $\mathcal{B} = \{b_{\mathrm{L}_0}, b_{\mathrm{L}_1}\}$ or $\{b_{\mathrm{N}_0}, b_{\mathrm{N}_1}\}$ or $\{b_{\mathrm{L}_0}, b_{\mathrm{N}_0}\}$ or $\{b_{\mathrm{N}_0}, b_{\mathrm{L}_0}\}$ depending on the rank of the BSs in terms of the RSS. In other words, the serving BSs are the first two BSs providing the strongest average RSSs. The different classifications of AUs are listed in Table I.

D. NOMA Model

We focus on a pair of typical AU and TU associating with the tagged BS. It is worth noting that an appropriate design of pairing strategy between AU and TU for NOMA is also important, which definitely will further enhance the NOMA performance. However, this is beyond the scope of this work and left for the future work. We assume that the AU and the TU are, respectively, the far user and the near user with the corresponding power control coefficients being ρ_{u} and ρ_{t}, where $\rho_{\mathrm{u}} + \rho_{\mathrm{t}} = 1$ and $\rho_{\mathrm{u}} > \rho_{\mathrm{t}}$. To maximize the received signal power at the typical AU, we consider the maximum ratio transmission (MRT) scheme, where the tagged BS is assumed to have the channel state information (CSI) between the tagged BS and the typical AU. Take a general v-th type BS b_i as an example. Define $\omega_{i,\mathrm{u}}$ and $\omega_{i,\mathrm{t}}$ as the Nakagami-m distributed small-scale fading from b_i to its associaed AU and TU, respectively. With MRT, the precoder

w_i of BS b_i is set as $\dfrac{\omega_{i,\mathrm{u}}^*}{|\omega_{i,\mathrm{u}}|}$, where $\omega_{i,\mathrm{u}}^*$ represents the complex conjugate of $\omega_{i,\mathrm{u}}$. To be specific, we use '0' and '1' to represent the typical AU and the typical TU, respectively. In addition, we define b_0 as the tagged BS and b_1 as the other cooperative BS if the typical AU is served as a CoMP AU. It is worth noting that b_0 and b_1 (if any) can be LoS or NLoS BS.

According to the above definition, the superimposed signal transmitted by the tagged BS b_0 and the cooperative BS b_1 (if any) is given by

$$s_0 = w_0 \omega_{0,0} \rho_\mathrm{u} \sqrt{P_\mathrm{t}} s_\mathrm{u} + w_0 \omega_{0,1} \rho_\mathrm{t} \sqrt{P_\mathrm{t}} s_\mathrm{t}, \tag{7}$$

$$s_1 = w_1 \omega_{1,0} \rho_\mathrm{u} \sqrt{P_\mathrm{t}} s_\mathrm{u} + w_1 \omega_{1,\mathrm{t}} \rho_\mathrm{t} \sqrt{P_\mathrm{t}} s_\mathrm{t}, \tag{8}$$

where $w_0 = \dfrac{\omega_{0,0}^*}{|\omega_{0,0}|}$ ($w_1 = \dfrac{\omega_{1,0}^*}{|\omega_{1,0}|}$) is the transmit precoder set by the tagged BS b_0 (the cooperative BS b_1, if any), $\omega_{0,0}$ ($\omega_{0,1}$) denotes the small-scale fading from the tagged BS b_0 to the typical AU (typical TU), and $\omega_{1,0}$ ($\omega_{1,\mathrm{t}}$) represents the small-scale fading from the cooperative BS b_1 to the typical AU (its associated TU, rather than the typical TU). Meanwhile, s_u and s_t are the information bearing for AU and TU, respectively, with $\mathbb{E}[|s_\mathrm{u}|^2] = \mathbb{E}[|s_\mathrm{t}|^2] = 1$.

We first consider the case when the typical AU is a Non-CoMP AU. In this case, the far user, i.e., the AU, decodes its message directly by treating the signal transmitted to the TU as interference, leading to the following SIR

$$\Upsilon_\mathrm{u}^\mathrm{NC} = \frac{\rho_\mathrm{u} P_\mathrm{t} \zeta_v(b_0) |\widetilde{\omega}_{0,0}|^2}{\rho_\mathrm{t} P_\mathrm{t} \zeta_v(b_0) |\widetilde{\omega}_{0,0}|^2 + \sum_{i \in \Phi_\mathrm{B} \backslash b_0} P_\mathrm{t} \zeta_v(b_i) |\widetilde{\omega}_{i,0}|^2}, \tag{9}$$

where $|\widetilde{\omega}_{0,0}|^2 \triangleq |w_0 \omega_{0,0}|^2 = |\omega_{0,0}|^2$ ($|\widetilde{\omega}_{i,0}|^2 \triangleq |w_i \omega_{i,0}|^2 = |\omega_{i,0}|^2$) represents the channel power gain between the tagged BS b_0 (interfering BS b_i) and the typical AU. Note that the first part in the denominator denotes the self-interference from the tagged BS due to the NOMA scheme between the typical AU and TU.

We then consider the case when the typical AU is a CoMP AU. In this case, the SIR at the AU can be expressed as

$$\Upsilon_\mathrm{u}^\mathrm{C} = \frac{|\sum_{k=0}^{1} (\rho_\mathrm{u} P_\mathrm{t} \zeta_v(b_k))^{\frac{1}{2}} \widetilde{\omega}_{k,0}|^2}{\sum_{k=0}^{1} \rho_\mathrm{t} P_\mathrm{t} \zeta_v(b_k) |\widetilde{\omega}_{k,0}|^2 + \sum_{i \in \Phi \backslash \mathcal{B}} P_\mathrm{t} \zeta_v(b_i) |\widetilde{\omega}_{i,0}|^2}, \tag{10}$$

where $\mathcal{B} = \{b_0, b_1\}$ denotes the cooperative BS set, $\widetilde{\omega}_{k,0} = w_k \omega_{k,0} = |\omega_{k,0}|$, $|\widetilde{\omega}_{k,0}|^2 = |\omega_{k,0}|^2$, $k \in \{0, 1\}$, and $|\widetilde{\omega}_{i,0}|^2 \triangleq |w_i \omega_{i,0}|^2 = |\omega_{i,0}|^2$, $i \in \Phi \backslash \mathcal{B}$. The first part of the denominator denotes the interference from the two cooperative BSs due to the NOMA scheme between the typical

AU and TU.

We finally derive the SIR expressions of the typical TU when forming a NOMA pair with a Non-CoMP AU and a CoMP AU, respectively. It is worth noting the small-scale fading from the tagged BS to the typical TU is independent of that from the tagged BS to the typical AU. Thus, the received SIR expression of the typical TU is the same, regardless of the type of the typical AU. Note that in this work, we assume perfect SIC at the typical TU, i.e., the message of the AU can be perfectly removed from the superimposed signal, and thus, the received SIR at the typical TU is given by

$$\Upsilon_{\mathrm{t}} = \frac{\rho_{\mathrm{t}} P_{\mathrm{t}} \zeta_{\mathrm{t}}(b_0) |\widetilde{\omega}_{0,1}|^2}{\sum_{j \in \Phi \backslash b_0} P_{\mathrm{t}} \zeta_{\mathrm{t}}(b_j) |\widetilde{\omega}_{j,1}|^2}, \tag{11}$$

where we define $|\widetilde{\omega}_{0,1}|^2 \triangleq |w_0 \omega_{0,1}|^2 = |\omega_{0,1}|^2$. With regards to the Rayleigh distribution, we have $|\widetilde{\omega}_{01}|^2 \sim \mathrm{Exp}(1)$.

For brevity of notation, we define the following symbols and functions, which will be used in the following analysis parts: $l_{\mathrm{L\_N}} \triangleq \left(\frac{\eta_{\mathrm{L}}}{\eta_{\mathrm{N}}} \right)^{\frac{1}{\alpha_{\mathrm{L}}}} (\Delta h_{\mathrm{u}})^{\frac{\alpha_{\mathrm{N}}}{\alpha_{\mathrm{L}}}}$, $l(r) = \sqrt{r^2 - (\Delta h_{\mathrm{u}})^2}$, $d_{\mathrm{L\_N}}(r) = \left(\frac{\eta_{\mathrm{N}}}{\eta_{\mathrm{L}}} \right)^{\frac{1}{\alpha_{\mathrm{N}}}} r^{\frac{\alpha_{\mathrm{L}}}{\alpha_{\mathrm{N}}}}$, and $d_{\mathrm{N\_L}}(r) = \left(\frac{\eta_{\mathrm{L}}}{\eta_{\mathrm{N}}} \right)^{\frac{1}{\alpha_{\mathrm{L}}}} r^{\frac{\alpha_{\mathrm{N}}}{\alpha_{\mathrm{L}}}}$.

III. RELEVANT DISTANCE AND USER ASSOCIATION ANALYSIS

To obtain the coverage probability and ergodic rate, in this section, we first derive the association probabilities when the typical AU is served as a Non-CoMP AU and CoMP AU, respectively. Then, the PDFs of the distance between the tagged BS (BSs) and the typical Non-CoMP AU (CoMP AU) are derived.

A. Relevant Distance Distributions

In this subsection, we derive the distribution of some relevant distances in Lemma 1 and Lemma 2, which will be used when deriving the association probabilities.

Lemma 1: The PDF of the distances between the typical Non-CoMP AU and the closest NLoS BS b_{N_0} and LoS BS b_{L_0}, denoted by $f_{R_{\mathrm{N}_0}}(r)$ and $f_{R_{\mathrm{L}_0}}(r)$, respectively, are given by

$$f_{R_{\mathrm{N}_0}}(r) = 2\pi \lambda_b r p^{\mathrm{N}}(r) \exp \left(-2\pi \lambda_b \int_0^{l(r)} z p^{\mathrm{N}}(z) dz \right), \tag{12}$$

$$f_{R_{\mathrm{L}_0}}(r) = 2\pi \lambda_b r p^{\mathrm{L}}(r) \exp \left(-2\pi \lambda_b \int_0^{l(r)} z p^{\mathrm{L}}(z) dz \right), \tag{13}$$

where $r \geq \Delta h_{\mathrm{u}}$, $p^{\mathrm{N}}(r) = 1 - p^{\mathrm{L}}(r)$ with $p^{\mathrm{L}}(r) = p^{\mathrm{L}}(z)\big|_{z=\sqrt{r^2-(\Delta h_{\mathrm{u}})^2}}$, $\lambda_b p^{\mathrm{N}}(r)$ and $\lambda_b p^{\mathrm{L}}(r)$ represent the intensities of the NLoS BS set $\Phi_{\mathrm{B}}^{\mathrm{N}}$, and LoS BS set $\Phi_{\mathrm{B}}^{\mathrm{L}}$, respectively.

Proof: The results can be proved by a modification of Lemma 1 in [37] for the cellular-connected UAV network, which is omitted due to space limitation. $\qquad\square$

Lemma 2: The joint PDF of the distances between the typical CoMP AU and the two cooperative BSs of the same type, denoted by $f_{R_{\mathrm{N}_0}, R_{\mathrm{N}_1}}(r_{\mathrm{N}_0}, r_{\mathrm{N}_1})$, and $f_{R_{\mathrm{L}_0}, R_{\mathrm{L}_1}}(r_{\mathrm{L}_0}, r_{\mathrm{L}_1})$, and of the different types, denoted by $f_{R_{\mathrm{N}_0}, R_{\mathrm{L}_0}}(r_{\mathrm{N}_0}, r_{\mathrm{L}_0})$, and $f_{R_{\mathrm{L}_0}, R_{\mathrm{N}_0}}(r_{\mathrm{L}_0}, r_{\mathrm{N}_0})$, are given by

$$f_{R_{\mathrm{N}_0}, R_{\mathrm{N}_1}}(r_{\mathrm{N}_0}, r_{\mathrm{N}_1}) = (2\pi\lambda_{\mathrm{b}})^2 r_{\mathrm{N}_0} r_{\mathrm{N}_1} p^{\mathrm{N}}(r_{\mathrm{N}_0}) p^{\mathrm{N}}(r_{\mathrm{N}_1}) \exp\left(-2\pi\lambda_{\mathrm{b}} \int_0^{l(r_{\mathrm{N}_1})} z p^{\mathrm{N}}(z) dz\right), \quad (14)$$

$$f_{R_{\mathrm{L}_0}, R_{\mathrm{L}_1}}(r_{\mathrm{L}_0}, r_{\mathrm{L}_1}) = (2\pi\lambda_{\mathrm{b}})^2 r_{\mathrm{L}_0} r_{\mathrm{L}_1} p^{\mathrm{L}}(r_{\mathrm{L}_0}) p^{\mathrm{L}}(r_{\mathrm{L}_1}) \exp\left(-2\pi\lambda_{\mathrm{b}} \int_0^{l(r_{\mathrm{L}_1})} z p^{\mathrm{L}}(z) dz\right), \quad (15)$$

$$f_{R_{\mathrm{N}_0}, R_{\mathrm{L}_0}}(r_{\mathrm{N}_0}, r_{\mathrm{L}_0}) = (2\pi\lambda_{\mathrm{b}})^2 r_{\mathrm{N}_0} r_{\mathrm{L}_0} p^{\mathrm{N}}(r_{\mathrm{N}_0}) p^{\mathrm{L}}(r_{\mathrm{L}_0}) \exp\left(-2\pi\lambda_{\mathrm{b}} \int_0^{l(r_{\mathrm{L}_0})} z p^{\mathrm{L}}(z) dz\right), \quad (16)$$

$$f_{R_{\mathrm{L}_0}, R_{\mathrm{N}_0}}(r_{\mathrm{L}_0}, r_{\mathrm{N}_0}) = \begin{cases} f_{R_{\mathrm{L}_0}}(r_{\mathrm{L}_0}) f_{R_{\mathrm{N}_0}}(r_{\mathrm{N}_0}), & \text{if } r_{\mathrm{L}_0} \in [\Delta h_{\mathrm{u}}, l_{\mathrm{L\_N}}), r_{\mathrm{N}_0} \geq \Delta h_{\mathrm{u}}, \\ (2\pi\lambda_b)^2 r_{\mathrm{L}_0} r_{\mathrm{N}_0} p^{\mathrm{L}}(r_{\mathrm{L}_0}) p^{\mathrm{N}}(r_{\mathrm{N}_0}) \\ \quad \times \exp\left(-2\pi\lambda_b \int_0^{l(r_{\mathrm{L}_0})} z p^{\mathrm{L}}(z) dz\right), & \text{if } r_{\mathrm{L}_0} \geq l_{\mathrm{L\_N}}, r_{\mathrm{N}_0} > d_{\mathrm{L\_N}}(r_{\mathrm{L}_0}), \end{cases} \quad (17)$$

where $r_{\mathrm{N}_1} > r_{\mathrm{N}_0} \geq \Delta h_{\mathrm{u}}$ in (14), $r_{\mathrm{L}_1} > r_{\mathrm{L}_0} \geq \Delta h_{\mathrm{u}}$ in (15), and $r_{\mathrm{L}_0} > r_{\mathrm{N}_0} \geq \Delta h_{\mathrm{u}}$ in (16). $f_{R_{\mathrm{N}_0}}(r_{\mathrm{N}_0})$ and $f_{R_{\mathrm{L}_0}}(r_{\mathrm{L}_0})$ are given by (12) and (13), respectively.

Proof: See Appendix A. $\qquad\square$

It is worth noting that the difference between $f_{R_{\mathrm{N}_0}, R_{\mathrm{L}0}}(r_{\mathrm{N}_0}, r_{\mathrm{L}_0})$, and $f_{R_{\mathrm{L}_0}, R_{\mathrm{N}_0}}(r_{\mathrm{L}_0}, r_{\mathrm{N}_0})$ lies in the fact that the BS providing the strongest average RSS for the typical AU is of the NLoS type in the former, and of the LoS type in the latter.

B. User Association Analysis

We define $\mathcal{A}_{\mathrm{L}_0}$ and $\mathcal{A}_{\mathrm{N}_0}$ as the probabilities when the typical Non-CoMP AU is associated with the nearest LoS BS and NLoS BS, respectively. We further define $\mathcal{A}_{\mathrm{L}_0,\mathrm{L}_1}$, $\mathcal{A}_{\mathrm{N}_0,\mathrm{N}_1}$, $\mathcal{A}_{\mathrm{L}_0,\mathrm{N}_0}$, and $\mathcal{A}_{\mathrm{N}_0,\mathrm{L}_0}$ as the probabilities when the typical CoMP AU is associated with $\{b_{\mathrm{L}_0}, b_{\mathrm{L}_1}\}$, $\{b_{\mathrm{N}_0}, b_{\mathrm{N}_1}\}$, $\{b_{\mathrm{L}_0}, b_{\mathrm{L}_1}\}$, and $\{b_{\mathrm{N}_0}, b_{\mathrm{L}_0}\}$, respectively.

Lemma 3: The probabilities of the typical Non-CoMP AU associated with the serving BS are

given by (18), (19), and of the typical CoMP AU associated with the two serving BSs for the four different cases are given by (20), (21), (22), and (23), respectively.

$$
\mathcal{A}_{L_0} = \int_{\Delta h_u}^{l_{L\_N}} \int_{\theta^{\frac{1}{\alpha_L}} r_{L_0}}^{+\infty} f_{R_{L_0},R_{L_1}}(r_{L_0},r_{L_1}) dr_{L_1} dr_{L_0}
$$
$$
+ \int_{l_{L\_N}}^{+\infty} \int_{\theta^{\frac{1}{\alpha_L}} r_{L_0}}^{+\infty} f_{R_{L_0},R_{L_1}}(r_{L_0},r_{L_1}) \exp\left(-2\pi\lambda_b \int_0^{l\left(\theta^{\frac{1}{\alpha_N}} d_{L\_N}(r_{L_0})\right)} z p^N(z) dz\right) dr_{L_1} dr_{L_0},
$$
(18)

$$
\mathcal{A}_{N_0} = \int_{\Delta h_u}^{+\infty} \int_{\theta^{\frac{1}{\alpha_N}} r_{N_0}}^{+\infty} \exp\left(-2\pi\lambda_b \int_0^{l\left(\theta^{\frac{1}{\alpha_L}} d_{N\_L}(r_{N_0})\right)} z p^N(z) dz\right) f_{R_{N_0},R_{N_1}}(r_{N_0},r_{N_1}) dr_{N_1} dr_{N_0},
$$
(19)

$$
\mathcal{A}_{L_0,L_1} = \int_{\Delta h_u}^{l_{L\_N}} \int_{r_{L_0}}^{\theta^{\frac{1}{\alpha_L}} r_{L_0}} f_{R_{L_0},R_{L_1}}(r_{L_0},r_{L_1}) dr_{L_1} dr_{L_0}
$$
$$
+ \int_{l_{L\_N}}^{+\infty} \int_{r_{L_0}}^{\theta^{\frac{1}{\alpha_L}} r_{L_0}} f_{R_{L_0},R_{L_1}}(r_{L_0},r_{L_1}) \exp\left(-2\pi\lambda_b \int_0^{l\left(\theta^{\frac{1}{\alpha_N}} d_{L\_N}(r_{L_0})\right)} z p^N(z) dz\right) dr_{L_1} dr_{L_0},
$$
(20)

$$
\mathcal{A}_{N_0,N_1} = \int_{\theta^{\frac{1}{\alpha_L}} l_{L\_N}}^{+\infty} \int_{\theta^{\frac{1}{\alpha_N}} \Delta h_u}^{d_{L\_N}(r_{L_0})} \int_{\frac{1}{\theta}^{\frac{1}{\alpha_N}} r_{N_1}}^{r_{N_1}} f_{R_{N_0},R_{N_1}}(r_{N_0},r_{N_1}) f_{R_{L_0}}(r_{L_0}) dr_{N_0} dr_{N_1} dr_{L_0},
$$
(21)

$$
\mathcal{A}_{L_0,N_0} = \int_{\frac{1}{\theta}^{\frac{1}{\alpha_L}} l_{L\_N}}^{l_{L\_N}} \int_{\Delta h_u}^{\theta^{\frac{1}{\alpha_N}} d_{L\_N}(r_{L_0})} \int_{d_{N\_L}(r_{N_0})}^{+\infty} f_{R_{L_0}}(r_{L_0}) f_{R_{N_0}}(r_{N_0}) f_{R_{L_1}}(r_{L_1}) dr_{L_1} dr_{N_0} dr_{L_0}
$$
$$
+ \int_{l_{L\_N}}^{+\infty} \int_{d_{L\_N}(r_{L_0})}^{\theta^{\frac{1}{\alpha_N}} d_{L\_N}(r_{L_0})} \int_{d_{N\_L}(r_{N_0})}^{+\infty} f_{R_{L_0},R_{N_0}}(r_{L_0},r_{N_0}) f_{R_{L_1}}(r_{L_1}) dr_{L_1} dr_{N_0} dr_{L_0},
$$
(22)

$$
\mathcal{A}_{N_0,L_0} = \int_{\Delta h_u}^{+\infty} \int_{d_{N\_L}(r_{N_0})}^{\theta^{\frac{1}{\alpha_L}} d_{N\_L}(r_{N_0})} \int_{d_{L\_N}(r_{L_0})}^{+\infty} f_{R_{N_0},R_{L_0}}(r_{N_0},r_{L_0}) f_{R_{N_1}}(r_{N_1}) dr_{N_1} dr_{L_0} dr_{N_0},
$$
(23)

where $f_{R_{N_1}}(r) = f_{R_{N_0}}(r)$, and $f_{R_{L_1}}(r) = f_{R_{L_0}}(r)$ are given by (12) and (13), respectively. The joint PDFs $f_{R_{N_0},R_{N_1}}(r_{N_0},r_{N_1})$, $f_{R_{L_0},R_{L_1}}(r_{L_0},r_{L_1})$, $f_{R_{N_0},R_{L_0}}(r_{N_0},r_{L_0})$, and $f_{R_{L_0},R_{N_0}}(r_{L_0},r_{N_0})$, are given by (14), (15), (16), and (17), respectively.

Proof: See Appendix B. □

With the above lemmas, we further derive the PDF of the distances between the typical Non-CoMP AU (CoMP AU) and the serving BS (two serving cooperative BSs) given that the typical Non-CoMP AU (CoMP AU) is associated with a LoS BS or NLoS BS (two LoS BSs, two NLoS BSs, or one LoS BS and one NLoS BS), respectively.

Lemma 4: Given that the typical Non-CoMP AU is associated with a LoS BS (NLoS BS), the

PDF of the distance between the typical Non-CoMP AU and the serving LoS BS (NLoS BS), denoted by $f_{\widetilde{R}_{L_0}}(r_{L_0}) \left(f_{\widetilde{R}_{N_0}}(r_{N_0}) \right)$, is given by

$$
f_{\widetilde{R}_{L_0}}(r_{L_0}) = \begin{cases} \frac{1}{\mathcal{A}_{L_0}} \int_{\theta^{\frac{1}{\alpha_L}} r_{L_0}}^{\infty} f_{R_{L_0},R_{L_1}}(r_{L_0},r_2) dr_2, & \text{if } r_{L_0} \in [\Delta h_u, l_{L\_N}), \\ \frac{1}{\mathcal{A}_{L_0}} \exp\left(-2\pi\lambda_b \int_0^{l(\widetilde{d}_{L\_N}(r_{L_0}))} z p^N(z) dz\right) \\ \qquad \times \int_{\theta^{\frac{1}{\alpha_L}} r_{L_0}}^{\infty} f_{R_{L_0},R_{L_1}}(r_{L_0},r_2) dr_2, & \text{if } r_{L_0} \geq l_{L\_N}, \end{cases} \tag{24}
$$

$$
f_{\widetilde{R}_{N_0}}(r_{N_0}) = \frac{1}{\mathcal{A}_{N_0}} \exp(-2\pi\lambda_b \int_0^{l\left(\theta^{\frac{1}{\alpha_L}} d_{N\_L}(r_{N_0})\right)} z p^L(z) dz) \int_{\theta^{\frac{1}{\alpha_L}} r_{N_0}}^{\infty} f_{R_{N_0},R_{N_1}}(r_{N_0},r_2) dr_2, \tag{25}
$$

where $r_{N_0} \geq \Delta h_u$ in (25), $f_{R_{N_0}}(r_{N_0})$ and $f_{R_{L_0}}(r_{L_0})$ are given by (12) and (13), respectively.

Proof: See Appendix C. □

Lemma 5: Given that the typical CoMP AU is associated with two cooperative BSs, i.e., $\mathcal{B} = \{b_{L_0}, b_{L_1}\}, \{b_{N_0}, b_{N_1}\}, \{b_{L_0}, b_{N_0}\}, \{b_{N_0}, b_{L_0}\}$, the PDFs of the distance between the typical CoMP AU and the corresponding cooperative BSs, denoted by $f_{\widetilde{R}_{L_0},\widetilde{R}_{L_1}}(r_{L_0},r_{L_1})$, $f_{\widetilde{R}_{N_0},\widetilde{R}_{N_1}}(r_{N_0},r_{N_1})$, $f_{\widetilde{R}_{L_0},\widetilde{R}_{N_0}}(r_{L_0},r_{N_0})$, $f_{\widetilde{R}_{N_0},\widetilde{R}_{L_0}}(r_{N_0},r_{L_0})$, are given by

$$
f_{\widetilde{R}_{L_0},\widetilde{R}_{L_1}}(r_{L_0},r_{L_1}) = \begin{cases} \frac{1}{\mathcal{A}_{L_0,L_1}} f_{R_{L_0},R_{L_1}}(r_{L_0},r_{L_1}), & \text{if } r_{L_0} \in [\Delta h_u, l_{L\_N}), r_{L_1} > r_{L_0}, \\ \frac{1}{\mathcal{A}_{L_0,L_1}} f_{R_{L_0},R_{L_1}}(r_{L_0},r_{L_1}) \\ \times \exp\left(-2\pi\lambda_b \int_0^{d_{L\_N}(r_{L_1})} z p^N(z) dz\right), & \text{if } r_{L_1} > r_{L_0} \geq l_{L\_N}, \end{cases} \tag{26}
$$

$$
f_{\widetilde{R}_{N_0},\widetilde{R}_{N_1}}(r_{N_0},r_{N_1}) = \frac{1}{\mathcal{A}_{N_0,N_1}} f_{R_{N_0},R_{N_1}}(r_{N_0},r_{N_1}) \exp\left(-2\pi\lambda_b \int_0^{d_{N\_L}(r_{N_1})} z p^N(z) dz\right), \tag{27}
$$

$$
f_{\widetilde{R}_{N_0},\widetilde{R}_{L_0}}(r_{N_0},r_{L_0}) = \frac{1}{\mathcal{A}_{N_0,L_0}} f_{R_{N_0},R_{L_0}}(r_{N_0},r_{L_0}) \exp\left(-2\pi\lambda_b \int_0^{d_{L\_N}(r_{L_0})} z p^N(z) dz\right), \tag{28}
$$

$$
f_{\widetilde{R}_{L_0},\widetilde{R}_{N_0}}(r_{L_0},r_{N_0}) = \begin{cases} \frac{1}{\mathcal{A}_{L_0,N_0}} f_{R_{L_0},R_{N_0}}(r_{L_0},r_{N_0}), & \text{if } r_{L_0} \in [\Delta h_u, l_{L\_N}), r_{N_0} \geq \Delta h_u, \\ \frac{1}{\mathcal{A}_{L_0,N_0}} f_{R_{L_0},R_{N_0}}(r_{L_0},r_{N_0}) \\ \times \exp\left(-2\pi\lambda_b \int_0^{d_{N\_L}(r_{N_1})} z p^N(z) dz\right), & \text{if } r_{L_0} \geq l_{L\_N}, r_{N_0} > d_{L\_N}(r_{L_0}), \end{cases} \tag{29}
$$

where $r_{N_1} > r_{N_0} \geq \Delta h_u$ in (27), $r_{L_0} > r_{N_0} \geq \Delta h_u$ in (28), $f_{R_{N_0},R_{N_1}}(r_{N_0},r_{N_1})$, $f_{R_{L_0},R_{L_1}}(r_{L_0},r_{L_1})$, $f_{R_{N_0},R_{L_0}}(r_{N_0},r_{L_0})$, and $f_{R_{L_0},R_{N_0}}(r_{L_0},r_{N_0})$, are given (14), (15), (16), and (17), respectively.

Proof: See Appendix D. □

IV. PERFORMANCE ANALYSIS

In this section, we focus on analyzing the system performance in terms of coverage probabilities of the typical AU and TU, and average ergodic rate for the proposed framework.

A. Coverage Probability

Since the typical AU is treated as the far user, the coverage probability is defined as the received SIR given by (8) and (9) (for the Non-CoMP AU and CoMP AU) is larger than the predefined SIR threshold T.

Theorem 1: Conditioned on associating with the closest NLoS BS b_{N_0} and LoS BS b_{L_0}, the DL coverage probabilities of the typical Non-CoMP AU adopting NOMA given the SIR threshold T, denoted by $\mathbb{P}_{N_0}(T)$ and $\mathbb{P}_{L_0}(T)$ are, respectively, given by

$$\mathbb{P}_{N_0}(T) = \int_{\Delta h_u}^{+\infty} \sum_{k=0}^{m_N-1} \frac{(-s)^k}{k!} \frac{\partial^k}{\partial s^k} \mathcal{L}_I(s)\Big|_{s=\frac{m_N T}{(\rho_u - \rho_t T)P_t \zeta_N(b_0)}} f_{\widetilde{R}_{N_0}}(r_{N_0}) dr_{N_0}, \tag{30}$$

$$\mathbb{P}_{L_0}(T) = \int_{\Delta h_u}^{l_{L\_N}} \sum_{k=0}^{m_L-1} \frac{(-s)^k}{k!} \frac{\partial^k}{\partial s^k} \widehat{\mathcal{L}}_I(s)\Big|_{s=\frac{m_L T}{(\rho_u - \rho_t T)P_t \zeta_L(b_0)}} f_{\widetilde{R}_{L_0}}(r_{L_0}) dr_{L_0}$$

$$+ \int_{l_{L\_N}}^{+\infty} \sum_{k=0}^{m_L-1} \frac{(-s)^k}{k!} \frac{\partial^k}{\partial s^k} \widetilde{\mathcal{L}}_I(s)\Big|_{s=\frac{m_L T}{(\rho_u - \rho_t T)P_t \zeta_L(b_0)}} f_{\widetilde{R}_{L_0}}(r_{L_0}) dr_{L_0}, \tag{31}$$

where $f_{\widetilde{R}_{L_0}}(r_{L_0})$ and $f_{\widetilde{R}_{N_0}}(r_{N_0})$ are the PDF of the corresponding distances given by (24) and (25), and the expressions of Laplace transform in (30) and (31) are, respectively, given by

$$\mathcal{L}_I(s) = \exp\left(-2\pi\lambda_b\left(\int_{l\left(\theta^{\frac{1}{\alpha_N}} r_{N_0}\right)}^{+\infty} C(s,z,m_N)zp^N(z)dz + \int_{l\left(\theta^{\frac{1}{\alpha_L}} d_{N\_L}(r_{N_0})\right)}^{+\infty} C(s,z,m_L)zp^L(z)dz\right)\right), \tag{32}$$

$$\widehat{\mathcal{L}}_I(s) = \exp\left(-2\pi\lambda_b\left(\int_0^\infty C(s,z,m_N)zp^N(z)dz + \int_{l(r_{L_0})}^\infty C(s,z,m_L)zp^L(z)dz\right)\right), \tag{33}$$

$$\widetilde{\mathcal{L}}_I(s) = \exp\left(-2\pi\lambda_b\left(\int_{l\left(\theta^{\frac{1}{\alpha_N}} d_{L\_N}(r_{L_0})\right)}^{+\infty} C(s,z,m_N)zp^N(z)dz + \int_{l(r_{L_0})}^\infty C(s,z,m_L)zp^L(z)dz\right)\right), \tag{34}$$

where we define $C(s,z,m_v) \triangleq 1 - \left(\frac{m_v}{m_v + s\eta_v\left(\sqrt{z^2 + \Delta h_u^2}\right)^{-\alpha_v}}\right)^{m_v}$, for $v \in \{L, N\}$.

Proof: The results can be proved by modifying the proof of Theorem 1 in [37] by incorporating the inter-user interference from NOMA for the cellular-connected UAV network, and omitted here due to space limitation. □

Theorem 2: Conditioned on associating with two cooperative BSs for the four different cases,

i.e., $\mathcal{B} = \{b_{L_0}, b_{L_1}\}, \{b_{N_0}, b_{N_1}\}, \{b_{L_0}, b_{N_0}\}$ and $\{b_{N_0}, b_{L_0}\}$, the coverage probabilities of the typical CoMP AU adopting NOMA given the SIR threshold T, are given by (35), (36), (37), and (38), respectively.

$$\mathbb{P}_{L_0,L_1}(T) \approx \int_{\Delta h_u}^{l_{L\_N}} \int_{r_{L_0}}^{\theta^{\frac{1}{\alpha_L}} r_{L_0}} \sum_{k=0}^{2m_L-1} \frac{(-s)^k}{k!} \frac{\partial^k}{\partial s^k} \widehat{\mathcal{L}}_I(s)|_{s=\frac{T}{(2\rho_u - \rho_t T)P_t\Theta}} f_{\widetilde{R}_{L_0},\widetilde{R}_{L_1}}(r_{L_0},r_{L_1})dr_{L_1}dr_{L_0}$$

$$+ \int_{l_{L\_N}}^{+\infty} \int_{r_{L_0}}^{\theta^{\frac{1}{\alpha_L}} r_{L_0}} \sum_{k=0}^{2m_L-1} \frac{(-s)^k}{k!} \frac{\partial^k}{\partial s^k} \widetilde{\mathcal{L}}_I(s)|_{s=\frac{T}{(2\rho_u - \rho_t T)P_t\Theta}} f_{\widetilde{R}_{L_0},\widetilde{R}_{L_1}}(r_{L_0},r_{L_1})dr_{L_1}dr_{L_0},$$

$$(35)$$

$$\mathbb{P}_{N_0,N_1}(T) \approx \int_{\Delta h_u}^{+\infty} \int_{r_{N_0}}^{\theta^{\frac{1}{\alpha_N}} r_{N_0}} \sum_{k=0}^{2m_N-1} \frac{(-s)^k}{k!} \frac{\partial^k}{\partial s^k} \mathcal{L}_I(s)|_{s=\frac{T}{(2\rho_u P_t - \rho_t P_t T)\Theta}} f_{\widetilde{R}_{N_0},\widetilde{R}_{N_1}}(r_{N_0},r_{N_1})dr_{N_1}dr_{N_0},$$

$$(36)$$

$$\mathbb{P}_{L_0,N_0}(T)$$

$$\approx \int_{\theta^{-\frac{1}{\alpha_L}} l_{L\_N}}^{l_{L\_N}} \int_{\Delta h_u}^{\theta^{\frac{1}{\alpha_N}} d_{L\_N}(r_{L_0})} \sum_{k=0}^{m_L+m_N-1} \frac{(-s)^k}{k!} \frac{\partial^k}{\partial s^k} \check{\mathcal{L}}_I(s)|_{s=\frac{T}{(2\rho_u - \rho_t T)P_t\Theta}} f_{\widetilde{R}_{L_0},\widetilde{R}_{N_0}}(r_{L_0},r_{N_0})dr_{N_0}dr_{L_0}$$

$$+ \int_{l_{L\_N}}^{+\infty} \int_{d_{L\_N}(r_{L_0})}^{\theta^{\frac{1}{\alpha_N}} d_{L\_N}(r_{L_0})} \sum_{k=0}^{m_L+m_N-1} \frac{(-s)^k}{k!} \frac{\partial^k}{\partial s^k} \ddot{\mathcal{L}}_I(s)|_{s=\frac{T}{(2\rho_u - \rho_t T)P_t\Theta}} f_{\widetilde{R}_{L_0},\widetilde{R}_{N_0}}(r_{L_0},r_{N_0})dr_{N_0}dr_{L_0},$$

$$(37)$$

$$\mathbb{P}_{N_0,L_0}(T)$$

$$= \int_{\Delta h_u}^{+\infty} \int_{d_{N\_L}(r_{N_0})}^{\theta^{\frac{1}{\alpha_L}} d_{N\_L}(r_{N_0})} \sum_{k=0}^{m_L+m_N-1} \frac{(-s)^k}{k!} \frac{\partial^k}{\partial s^k} \overline{\mathcal{L}}_I(s)|_{s=\frac{T}{(2\rho_u P_t - \rho_t P_t T)\Theta}} f_{\widetilde{R}_{N_0},\widetilde{R}_{L_0}}(r_{N_0},r_{L_0})dr_{L_0}dr_{N_0},$$

$$(38)$$

where the expressions of Laplace transform are given by

$$\widehat{\mathcal{L}}_I(s) = \exp\left(-2\pi\lambda_b\left(\int_0^\infty C(s,z,m_N)zp^N(z)dz + \int_{l(r_{L_1})}^\infty C(s,z,m_L)zp^L(z)dz\right)\right), \quad (39)$$

$$\widetilde{\mathcal{L}}_I(s) = \exp\left(-2\pi\lambda_b\left(\int_{l(d_{L\_N}(r_{L_1}))}^{+\infty} C(s,z,m_N)zp^N(z)dz + \int_{l(r_{L_1})}^\infty C(s,z,m_L)zp^L(z)dz\right)\right),$$

$$(40)$$

$$\mathcal{L}_I(s) = \exp\left(-2\pi\lambda_b\left(\int_{l(d_{N\_L}(r_{N_1}))}^{+\infty} C(s,z,m_N)zp^N(z)dz + \int_{l(r_{N_1})}^\infty C(s,z,m_L)zp^L(z)dz\right)\right),$$

$$(41)$$

$$\check{\mathcal{L}}_I(s) = \exp\left(-2\pi\lambda_b\left(\int_0^{+\infty} C(s,z,m_N)zp^N(z)dz + \int_{l(d_{N\_L}(r_{N_0}))}^{+\infty} C(s,z,m_L)zp^L(z)dz\right)\right),$$

$$(42)$$

$$\ddot{\mathcal{L}}_I(s) = \exp\left(-2\pi\lambda_b\left(\int_{l(r_{N_0})}^{+\infty} C(s, z, m_N)zp^N(z)dz + \int_{l\left(d_{N\_L}(r_{N_0})\right)}^{+\infty} C(s, z, m_L)zp^L(z)dz\right)\right),$$
(43)

$$\overline{\mathcal{L}}_I(s) = \exp\left(-2\pi\lambda_b\left(\int_{l\left(d_{L\_N}(r_{L_0})\right)}^{+\infty} C(s, z, m_N)zp^N(z)dz + \int_{l(r_{L_0})}^{+\infty} C(s, z, m_L)zp^L(z)dz\right)\right),$$
(44)

where we define $C(s, z, m_v) \triangleq 1 - \left(\dfrac{m_v}{m_v + s\eta_v\left(\sqrt{z^2 + \Delta h_u^2}\right)^{-\alpha_v}}\right)^{m_v}$, for $v \in \{L, N\}$.

Proof: See Appendix E. $\qquad\qquad\qquad\qquad\qquad\qquad\qquad\qquad\qquad\qquad\qquad\square$

According to the law of total probability, the overall coverage probability of the typical CoMP AU adopting NOMA given the SIR threshold T can be expressed as

$$\mathbb{P}_u(T) = \mathcal{A}_{L_0}\mathbb{P}_{L_0}(T) + A_{N_0}\mathbb{P}_{N_0}(T) + \mathcal{A}_{L_0,L_1}\mathbb{P}_{L_0,L_1}(T)$$
$$+ \mathcal{A}_{N_0,N_1}\mathbb{P}_{N_0,N_1}(T) + \mathcal{A}_{L_0,N_0}\mathbb{P}_{L_0,N_0}(T) + \mathcal{A}_{N_0,L_0}\mathbb{P}_{N_0,L_0}(T).$$
(45)

By substituting the expressions of association probabilities in Lemma 3, and the coverage probabilities given in Theorem 1 and Theorem 2 into (45), we can derive the coverage probability of the typical AU.

Note that the typical TU is treated as the near user in this work, its coverage probability is defined as the received SIR given by (10) is larger than the predefined SIR threshold T, which is given by the following corollary.

Corollary 1: The coverage probability of the typical TU is given by

$$\mathbb{P}_t(T) = 2\pi\lambda_b \int_{\Delta h_t}^{+\infty} r \exp\left(-2\pi\lambda_b \int_r^{+\infty} (\frac{1}{1 + (\frac{\rho_t}{T})(\frac{x}{r})^{\alpha_t}})x dx - \pi\lambda_b(r^2 - \Delta h_t^2)\right) dr.$$
(46)

Proof: The result can be proved by a minor modification of Theorem 1 in [36], where we consider the NOMA scheme for TU. $\qquad\qquad\qquad\qquad\qquad\qquad\qquad\qquad\square$

B. Average Ergodic Rate of the Proposed CoMP-NOMA Scheme

In this subsection, we derive the average ergodic rate to evaluate the network performance in terms of the spectral efficiency for the proposed CoMP-NOMA scheme in the cellular-connected UAV network. To be specific, we first define the average achievable rates for the typical Non-CoMP AU, CoMP AU, and TU as

$$\mathcal{R}_u^{NC} \triangleq \mathbb{E}_\mathcal{B}\left[\mathbb{E}_{\Upsilon_u^{NC}}\left[\log_2\left(1 + \Upsilon_u^{NC}\right)\right]\right], \quad \mathcal{R}_u^C \triangleq \mathbb{E}_\mathcal{B}\left[\mathbb{E}_{\Upsilon_u^C}\left[\log_2\left(1 + \Upsilon_u^C\right)\right]\right],$$
(47)

$$\mathcal{R}_t \triangleq \mathbb{E}_{\Upsilon_t}\left[\log_2\left(1 + \Upsilon_t\right)\right].$$
(48)

Theorem 3: The average achievable rates for the typical Non-CoMP AU, CoMP AU, and TU are given by

$$\mathcal{R}_\mathrm{u}^\mathrm{NC} = \mathcal{A}_{\mathrm{L}_0} \mathcal{R}_\mathrm{u}^\mathrm{NC}(\mathcal{B} = \{b_{\mathrm{L}_0}\}) + \mathcal{A}_{\mathrm{N}_0} \mathcal{R}_\mathrm{u}^\mathrm{NC}(\mathcal{B} = \{b_{\mathrm{N}_0}\}), \tag{49}$$

$$\mathcal{R}_\mathrm{u}^\mathrm{C} = \mathcal{A}_{\mathrm{L}_0,\mathrm{L}_1} \mathcal{R}_\mathrm{u}^\mathrm{C}(\mathcal{B} = \{b_{\mathrm{L}_0}, b_{\mathrm{L}_1}\}) + \mathcal{A}_{\mathrm{N}_0,\mathrm{N}_1} \mathcal{R}_\mathrm{u}^\mathrm{C}(\mathcal{B} = \{b_{\mathrm{N}_0}, b_{\mathrm{N}_1}\})$$
$$+ \mathcal{A}_{\mathrm{L}_0,\mathrm{N}_0} \mathcal{R}_\mathrm{u}^\mathrm{C}(\mathcal{B} = \{b_{\mathrm{L}_0}, b_{\mathrm{N}_0}\}) + \mathcal{A}_{\mathrm{N}_0,\mathrm{L}_0} \mathcal{R}_\mathrm{u}^\mathrm{C}(\mathcal{B} = \{b_{\mathrm{N}_0}, b_{\mathrm{L}_0}\}), \tag{50}$$

$$\mathcal{R}_\mathrm{t} = 2\pi\lambda_b \int_0^{+\infty} \int_{\Delta h_\mathrm{t}}^{+\infty} r \exp\left(-2\pi\lambda_b \int_r^{+\infty} (\frac{1}{1+(\frac{\rho_t}{T})(\frac{x}{r})^{\alpha_t}})x dx - \pi\lambda_b(r^2 - \Delta h_\mathrm{t}^2)\right) dr d\tau, \tag{51}$$

where the association probabilities are given by Lemma 3, and the conditional average achievable rates are given by

$$\mathcal{R}_\mathrm{u}^\mathrm{NC}(\mathcal{B} = \{b_{\mathrm{L}_0}\}) = \int_0^{+\infty} \mathbb{P}_{\mathrm{L}_0}(2^\tau - 1)d\tau, \quad \mathcal{R}_\mathrm{u}^\mathrm{NC}(\mathcal{B} = \{b_{\mathrm{N}_0}\}) = \int_0^{+\infty} \mathbb{P}_{\mathrm{N}_0}(2^\tau - 1)d\tau, \tag{52}$$

$$\mathcal{R}_\mathrm{u}^\mathrm{C}(\mathcal{B} = \{b_{\mathrm{L}_0}, b_{\mathrm{L}_1}\}) = \int_0^{+\infty} \mathbb{P}_{\mathrm{L}_0,\mathrm{L}_1}(2^\tau - 1)d\tau, \quad \mathcal{R}_\mathrm{u}^\mathrm{C}(\mathcal{B} = \{b_{\mathrm{N}_0}, b_{\mathrm{N}_1}\}) = \int_0^{+\infty} \mathbb{P}_{\mathrm{N}_0,\mathrm{N}_1}(2^\tau - 1)d\tau,$$

$$\mathcal{R}_\mathrm{u}^\mathrm{C}(\mathcal{B} = \{b_{\mathrm{L}_0}, b_{\mathrm{N}_0}\}) = \int_0^{+\infty} \mathbb{P}_{\mathrm{L}_0,\mathrm{N}_0}(2^\tau - 1)d\tau, \quad \mathcal{R}_\mathrm{u}^\mathrm{C}(\mathcal{B} = \{b_{\mathrm{N}_0}, b_{\mathrm{L}_0}\}) = \int_0^{+\infty} \mathbb{P}_{\mathrm{N}_0,\mathrm{L}_0}(2^\tau - 1)d\tau, \tag{53}$$

with the conditional coverage probabilities within (52) and (53) being given by Theorem 1.

Proof. The results can be proved by substituting $T \triangleq 2^\tau - 1$ into the conditional coverage probabilities given in Theorem 2, and then integrating over the variable τ. We omit the proof here due to space limitation. ☐

According to the law of total probability, the average ergodic rate of the proposed CoMP-NOMA scheme is given by

$$\mathcal{R} = \mathcal{R}_\mathrm{u}^\mathrm{NC} + \mathcal{R}_\mathrm{u}^\mathrm{C} + \mathcal{R}_\mathrm{t}. \tag{54}$$

By substituting $\mathcal{R}_\mathrm{u}^\mathrm{NC}$, $\mathcal{R}_\mathrm{u}^\mathrm{C}$ and $\mathcal{R}_\mathrm{t}$ given in (49), (50), and (51) into (54), we can derive the average ergodic rate.

V. SIMULATIONS AND NUMERICAL RESULTS

In this section, we first verify the validity of the proposed framework by means of simulations, and then show the effectiveness of the proposed CoMP-NOMA scheme in terms of coverage probability and average ergodic rate. To show the superiority of the proposed CoMP-NOMA scheme, we compare with three benchmark schemes, namely, CoMP-OMA scheme, NOMA-Only

TABLE II
NUMERICAL AND SIMULATION PARAMETERS

Parameter	Description	Value
$\alpha_{\mathrm{L}}, \alpha_{\mathrm{N}}, \alpha_{\mathrm{t}}$	Pathloss exponents for LoS, NLoS and TU links	2.6, 3, 3
$A_{\mathrm{L}}, A_{\mathrm{N}}, A_{\mathrm{t}}$	Pathloss constants for LoS, NLoS, and TU links	-35 dB, -40 dB, -28.4 dB
$m_{\mathrm{L}}, m_{\mathrm{N}}$	Nakagami-m parameters for LoS and NLoS links	3, 1
P_{t}	Transmit power of BS	26 dB
λ_{b}	Density of BSs	10 km^{-2}
$\rho_{\mathrm{u}}, \rho_{\mathrm{t}}$	Power control coefficients for AU and TU	0.9, 0.1
θ	Cooperation threshold	4 dB
$h_{\mathrm{u}}, h_{\mathrm{b}}, h_{\mathrm{t}}$	Altitudes of AU, BS and TU	75 m, 19 m, 1.5 m
B, C	Air-to-Ground channel parameters	9.61, 0.16

scheme, and OMA-Only scheme. To make a fair comparison, for the OMA in both CoMP-OMA scheme and OMA-Only scheme, the tagged BS allocates half unit of resource, and transmits with half of its power budget to both the typical AU and the typical TU, respectively [38]. While for the NOMA-Only scheme, all AUs are served as non-COMP AUs.

A. Analytical Framework Validation

In this work, we employ the Gamma approximation and the Cauchy-Schwarz's inequality in the analytical computation of coverage probability in Theorem 2. To verify the feasibility of these approximations, we consider a horizontal area of 10000×10000 m^2 with 10^5 iterations in the simulation. The horizontal locations of BSs, AUs, and TUs are a realization of three independent PPPs of densities λ_{b}, λ_{u} and λ_{t}, with λ_{t}=10λ_{u}=100λ_{b}. Unless stated otherwise, we use the simulation parameters as listed in Table II.

In Fig. 2, we depict the association probabilities of AU as a function of AU's altitude for different association cases. It can be seen that the analytical results perfectly match the simulation results, which validates the accuracy of the obtained analysis in Lemma 3. We observe that $\mathcal{A}_{\mathrm{L}_0}$ exhibits the concave behavior as a function of AU's altitude h_u, and $\mathcal{A}_{\mathrm{L}_0,\mathrm{L}_1}$ grows with the increasing h_{u}, while the probabilities of the other four association cases $\mathcal{A}_{\mathrm{N}_0}$, $\mathcal{A}_{\mathrm{N}_0,\mathrm{N}_1}$, $\mathcal{A}_{\mathrm{L}_0,\mathrm{N}_1}$, and $\mathcal{A}_{\mathrm{N}_0,\mathrm{L}_1}$ decline with the increasing h_{u} and reduce to zero when h_{u} is greater than 120 m. This is because with the increase of h_{u}, the LoS probability of AU grows which enlarges the probability to associate with the LoS BS. However, as h_{u} further grows, $\mathcal{A}_{\mathrm{L}_0}$ decreases while $\mathcal{A}_{\mathrm{L}_0,\mathrm{L}_1}$ increases. This is because the ratio of RSS from the nearest LoS BS to that from
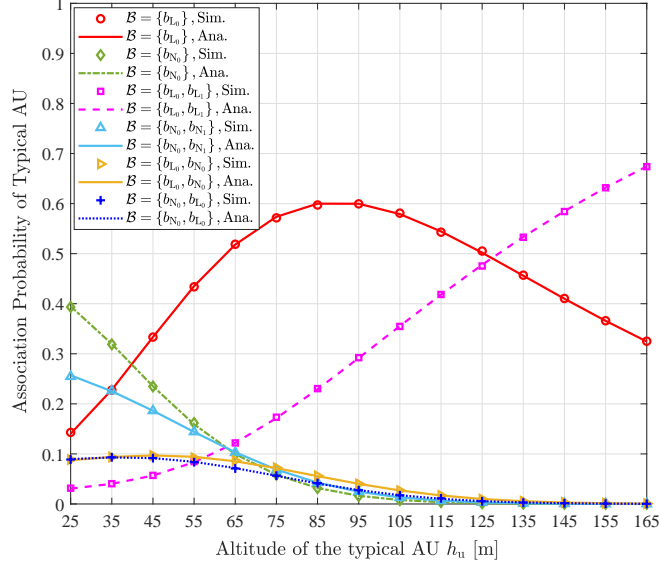
Fig. 2.   Association probabilities of the typical AU as a function of AU's altitude for different association cases.
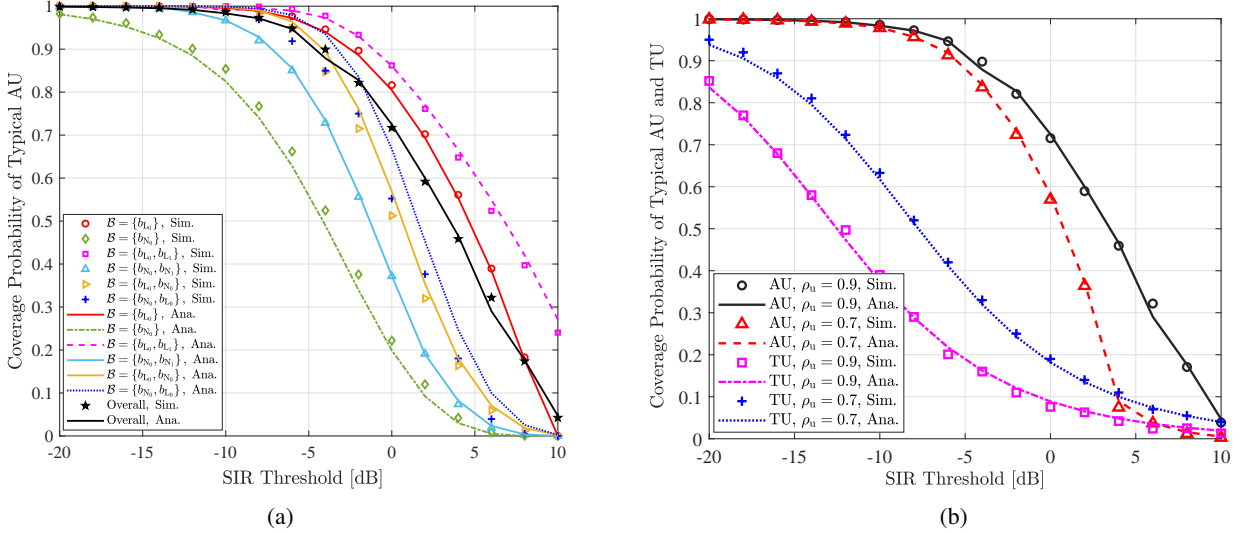

Fig. 3.   (a) Conditional and overall coverage probabilities of the typical AU as a function of SIR threshold, (b) coverage probability of the typical AU and TU as a function of SIR threshold for different power control coefficient ρ_{u}.

the dominant interfering BS declines, enlarging the cooperative probability. What's more, the gradually growing h_{u} results in the higher LoS probability, leading to the higher $\mathcal{A}_{\mathrm{L}_0,\mathrm{L}_1}$.

In Fig. 3, we verify the accuracy of coverage probabilities of the typical AU and TU by varying SIR threshold and power control coefficient. Fig. 3(a) shows a good match between the simulations and the theoretical analysis for most of cases except for the cases $\mathcal{B} = \{b_{\mathrm{N}_0}, b_{\mathrm{L}_0}\}$
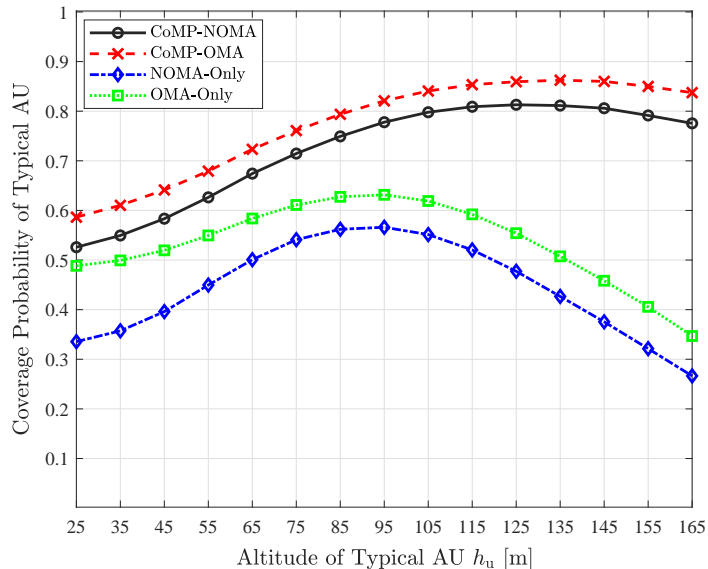
Fig. 4. Comparison of the typical AU's coverage probability for different schemes as a function of AU's altitude.

and $\mathcal{B} = \{b_{L_0}, b_{N_0}\}$. The gap is due to the use of Gamma approximation and Cauchy-Schwarz's inequality in the computation of conditional coverage probability. However, since the occurrence probability of these two cases is small, the gap has little impact on the overall coverage probability. Associating with two LoS BSs (only one NLoS BS) achieves the largest (lowest) coverage for the AU. What's more, the only one LoS BS association case is the second largest, higher than the cooperation case with one LoS BS and one NLoS BS. This is because the only one LoS BS association case means that the largest RSS is sufficiently large, while the cooperation case means that the first two largest RSSs are comparable. Fig. 3(b) shows a good match between the simulations and analytical results, which verifies the correctness of the coverage probabilities for both the typical AU and TU. What's more, we observe that increasing ρ_u is beneficial to AU's coverage probability while aggravating the TU's coverage probability. This is due to the fact that allocating more transmit power to the typical AU enhances its received SIR.

B. Coverage Probability Evaluation

In Fig. 4, we evaluate the coverage probability of AU as a function of AU's altitude under different schemes. We observe that the coverage probability achieved by the proposed CoMP-NOMA scheme is higher than that achieved by NOMA-Only scheme and OMA-Only scheme, while a little lower than that achieved by the CoMP-OMA scheme. This is due to the enhanced
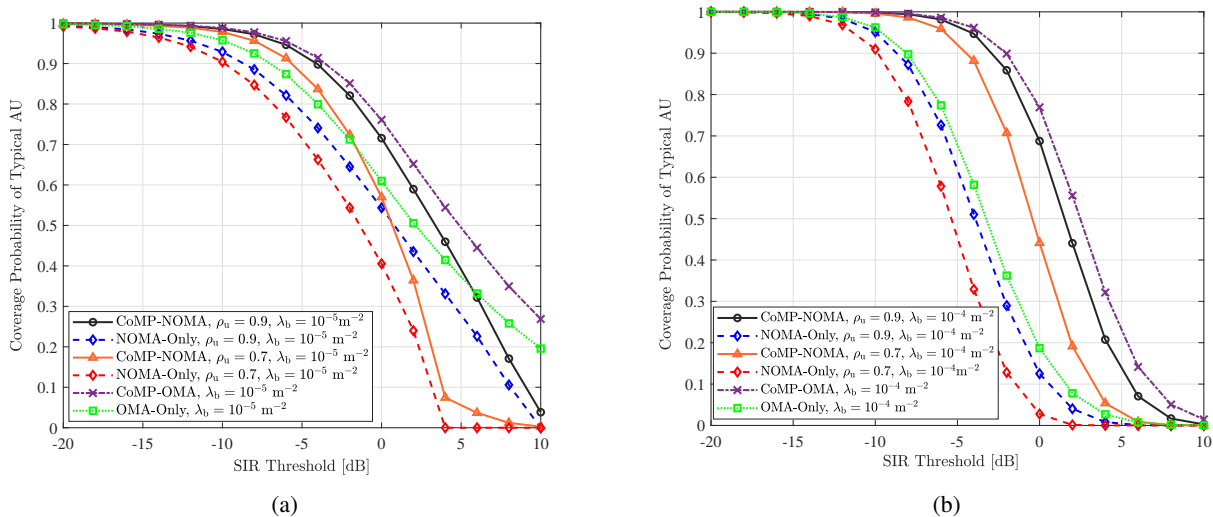
Fig. 5. Comparison of the typical AU's coverage probability for different schemes as a function of SIR threshold, where (a) is for $\lambda_{\text{b}} = 10^{-5}$ m^{-2}, and (b) is for $\lambda_b = 10^{-4}$ m^{-2}.

SIR achieved by CoMP, and the inter-user interference caused by NOMA. What's more, the coverage probability first grows and then declines as a function of the AU's altitude. The augmented coverage probability in the initial stage is due to the growing LoS probability of the A2G link and thus the received SIR, while the decreasing coverage probability in the later stage can be explained by the fact that the incremental path loss overweighs the gain from the increasing LoS probability. Therefore, the proposed framework allows to derive the optimal AU's altitude to achieve the largest coverage probability for AU.

In Fig. 5, we compare the typical AU's coverage probability for different schemes as a function of SIR threshold with different power control coefficient ρ_{u} and BS density λ_{b}. For both Fig. 5(a) and Fig. 5(b), we observe that the COMP-OMA scheme achieves the highest coverage probability, while the NOMA-Only scheme with ρ_{u}=0.7 achieves the lowest coverage probability. Allocating more power budget to AU in both CoMP-NOMA scheme and NOMA-Only scheme is beneficial to AU's coverage probability. For a smaller BS density $\lambda_{\text{b}} = 10^{-5}$ m^{-2}, Fig. 5(a) shows that ρ_{u} has larger effect for a higher SIR threshold. That's why the typical AU's coverage probability achieved by COMP-NOMA scheme with ρ_{u}=0.7 is lower than that achieved by NOMA-Only scheme with ρ_{u}=0.9 and OMA-Only scheme when the SIR threshold increases to a certain extent. Yet, for a larger BS density $\lambda_{\text{b}} = 10^{-4}$ m^{-2}, we observe that there is no crossing between curves. This is because the network is interference-limited in the dense network scenario, which highlights the benefit of BS cooperation in reducing the dominated interferer.
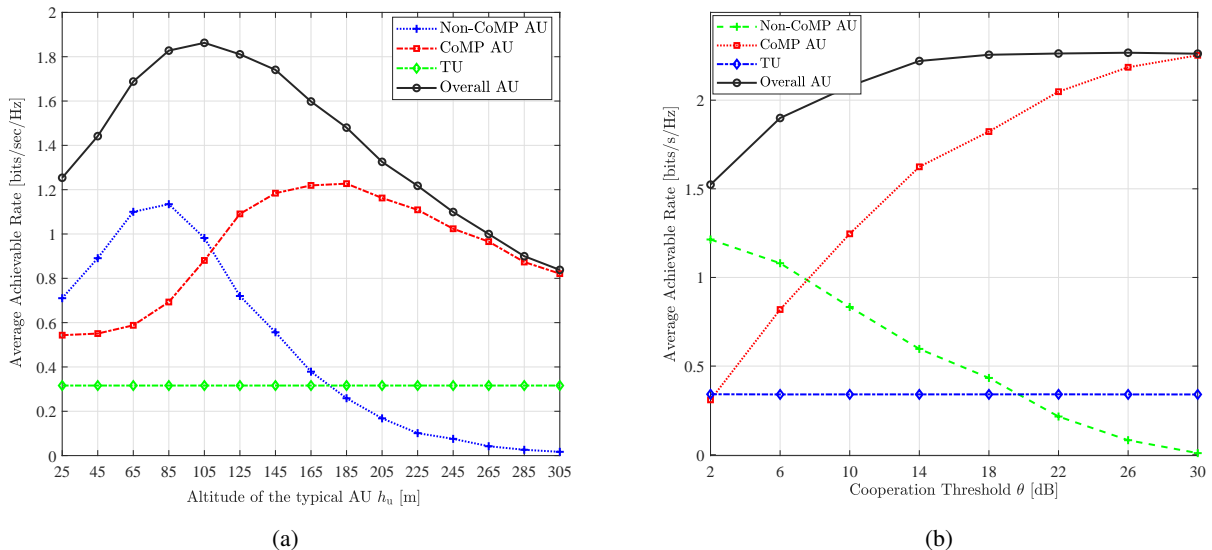
Fig. 6. Average achievable rate for CoMP AU, non-CoMP AU, Overall AU, and TU by varying (a) AU's altitude, and (b) cooperation threshold θ.

C. Average Ergodic Rate Evaluation

In Fig. 6, we depict the average achievable rates of the typical Non-CoMP AU ($\mathcal{R}_\mathrm{u}^\mathrm{NC}$), CoMP AU ($\mathcal{R}_\mathrm{u}^\mathrm{C}$), Overall AU ($\mathcal{R}_\mathrm{u}^\mathrm{NC}+\mathcal{R}_\mathrm{u}^\mathrm{C}$), and typical TU ($\mathcal{R}_\mathrm{t}$) given in Theorem 3 as a function of the typical AU's altitude h_u and the cooperation threshold θ, respectively. In Fig. 6(a), as h_u grows, we observe that $\mathcal{R}_\mathrm{u}^\mathrm{NC}$ and $\mathcal{R}_\mathrm{u}^\mathrm{C}$ increase first and then decrease, leading to the same trend of $\mathcal{R}_\mathrm{u}^\mathrm{NC}+\mathcal{R}_\mathrm{u}^\mathrm{C}$, while $\mathcal{R}_\mathrm{t}$ keeps unchanged. The variation of $\mathcal{R}_\mathrm{u}^\mathrm{NC}$ and $\mathcal{R}_\mathrm{u}^\mathrm{C}$ is due to the tradeoff between the incremental LoS probability for A2G link and the enlarging path loss. When h_u achieves 305 m, we observe that only CoMP AUs contribute to the rate. This can be explained by the fact that as h_u rises, the first two largest average RSSs become more comparable, increasing the probability of being a CoMP AU. The unchanged curve for $\mathcal{R}_\mathrm{t}$ can be explained by the assumption of perfect SIC conducted by TU, which eliminates the inter-user interference in NOMA. In Fig. 6(b), as θ increases, we observe that $\mathcal{R}_\mathrm{u}^\mathrm{NC}$ decreases and $\mathcal{R}_\mathrm{u}^\mathrm{C}$ increases, leading to an increase in $\mathcal{R}_\mathrm{u}^\mathrm{NC}+\mathcal{R}_\mathrm{u}^\mathrm{C}$. This is due to the fact that a higher θ enlarges the probability of being a CoMP AU. When θ grows to a certain value, e.g., 18 dB in this example, nearly all AUs are CoMP AUs, leading to a convergence of the overall rate.

In Fig. 7, we demonstrate the effectiveness of the proposed CoMP-NOMA scheme in terms of the average ergodic rate $\mathcal{R}$ in (54) by varying the altitude of the typical AU h_u and cooperation threshold θ, respectively. In Fig. 7(a), we observe that the ergodic rate achieved by the proposed
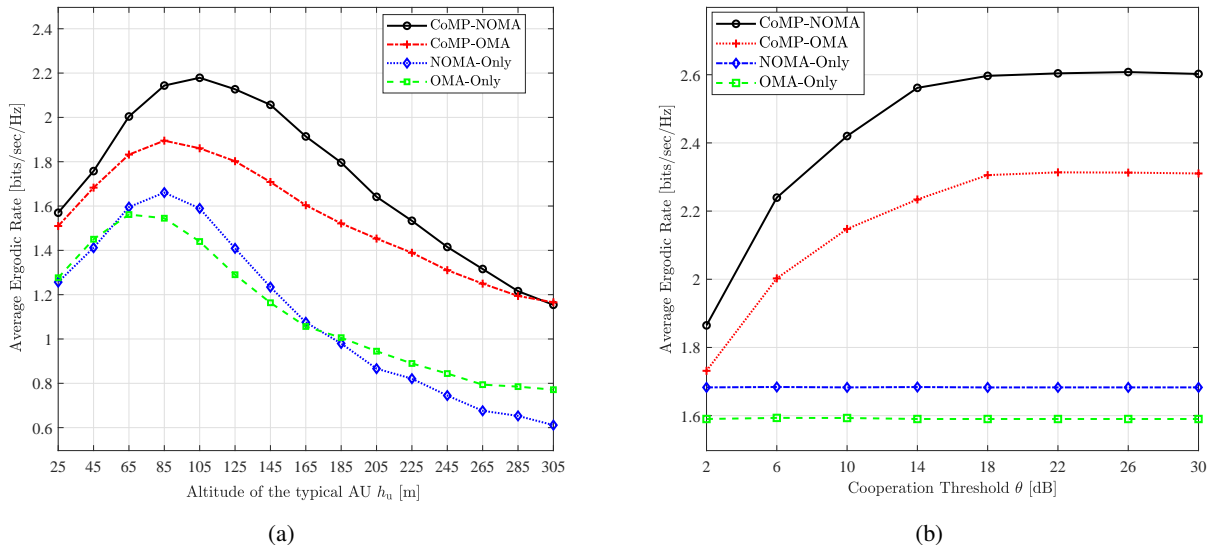
Fig. 7. Average achievable rate for different schemes by varying (a) AU's altitude, and (b) cooperation threshold θ.

CoMP-NOMA scheme is the largest, which is more superior for an appropriate h_{u}. What's more, we observe that the OMA-Only scheme may achieve the same or even higher ergodic rate than the NOMA-Only scheme when h_{u} is small or larger than a certain value. This can be explained by the fact that the inter-user interference in NOMA has a great impact on the typical AU, which is even obvious for a higher altitude. It shows that an appropriate setting of AU's altitude is beneficial to maximize the gain achieved by the proposed COMP-NOMA scheme. Fig. 7(b) shows that $\mathcal{R}$ achieved by CoMP-NOMA scheme and CoMP-OMA scheme both grow with θ, and converge when θ increases to a certain value, while $\mathcal{R}$ keeps unchanged for both NOMA-Only scheme and OMA-Only scheme. This is because when θ grows, the probability of the typical AU being a CoMP AU increases, harvesting more gain from the BS cooperation. When the probability of being a CoMP AU approaches to 1, the average ergodic rate converges to a constant value. Since there is no BS cooperation in NOMA-Only scheme and OMA-Only scheme, θ has no effect on $\mathcal{R}$. Although increasing the CoMP probability is beneficial to boost the average ergodic rate of the system, it also enlarges the cooperation overhead of the system. Our proposed analytical framework can be used to determine an appropriate cooperation threshold to maximize the ergodic rate while maintaining a relatively lower cooperation overhead.

VI. CONCLUSION

In this work, we proposed an interference-aware CoMP-NOMA scheme for cellular-connected UAV networks by considering the harmonious coexist of AUs and TUs. In this scheme, we exploited the BS cooperation gain for the qualified AUs by considering the CoMP scheme, while NOMA scheme was employed to enable the nonorthogonal transmissions for AUs and TUs by leveraging SIC. We first designed the classification rule for AUs, and the rule of NOMA cluster formulation for AUs and TUs. We then proposed an analytical framework to evaluate the coverage probability and spectral efficiency of the proposed CoMP-NOMA scheme. The superiority of the proposed CoMP-NOMA scheme has been demonstrated by comparing with three benchmark schemes. Our results showed that the proposed scheme can enhance the reliability of AUs through CoMP, and improve the spectral efficiency through NOMA as well. This work can be extended by considering the design of NOMA pairing strategy to further enhance the network performance, and including the cooperation overhead evaluation to enrich the analytical framework.

APPENDIX

A. *Proof of Lemma 2*

For the typical CoMP AU, there exists four cases for the cooperative BS set $\mathcal{B}$. We first consider the case $\mathcal{B} = \{b_{N_0}, b_{N_1}\}$, and define R_{N_0}, and R_{N_1} as the 3D distances between the typical CoMP AU and the first two nearest NLoS BSs within Φ^{N_B}, respectively. Meanwhile, $f_{R_{N_0}, R_{N_1}}(r_{N_0}, r_{N_1})$ is defined as the joint PDF of the distances. By definition, we have

$$f_{R_{N_0}, R_{N_1}}(r_{N_0}, r_{N_1}) = f_{R_{N_1}|R_{N_0}}(r_{N_1}|r_{N_0}) f_{R_{N_0}}(r_{N_0}), \quad r_{N_1} > r_{N_0} \geq \Delta h_{\mathrm{u}}, \tag{55}$$

where the conditional PDF in the righthand is given by

$$f_{R_{N_1}|R_{N_0}}(r_{N_1}|r_{N_0}) = 2\pi \lambda_b r_{N_1} p^{N}(r_{N_1}) \exp\left(-2\pi \lambda_b \left(\int_0^{l(r_{N_1})} z p^{L}(z) dz - \int_0^{l(r_{N_0})} z p^{L}(z) dz\right)\right). \tag{56}$$

By substituting (56) into (55), we complete the proof of $f_{R_{N_0}, R_{N_1}}(r_{N_0}, r_{N_1})$ in (14). Following the same steps as of $f_{R_{N_0}, R_{N_1}}(r_{N_0}, r_{N_1})$, we can complete the proof of $f_{R_{L_0}, R_{L_1}}(r_{L_0}, r_{L_1})$, $f_{R_{N_0}, R_{L_0}}(r_{N_0}, r_{L_0})$, and $f_{R_{L_0}, R_{N_0}}(r_{L_0}, r_{N_0})$, given by (15), (16), and (17), respectively.

B. Proof of Lemma 3

The probability of the typical Non-CoMP AU being associated with $\{b_{L_0}\}$ is given by

$$
\begin{aligned}
\mathcal{A}_{L_0} = \Pr\left[\mathcal{B} = \{b_{L_0}\}\right] &= \mathbb{E}_{R_{L_0}}\left[\Pr\left(\frac{\eta_L R_{L_0}^{-\alpha_L}}{\eta_{I_n} R_{I_n}^{-\alpha_{I_n}}} \geq \theta\right)\right] \\
&= \int_{\Delta h_u}^{+\infty} \Pr\left[R_{L_1} \geq \theta^{\frac{1}{\alpha_L}} R_{L_0}\right] \Pr\left[R_{N_0} \geq (\theta\frac{\eta_N}{\eta_L})^{\frac{1}{\alpha_N}} R_{L_0}^{\frac{\alpha_L}{\alpha_N}}\right] f_{R_{L_0}}(r_{L_0})dr_{L_0} \\
&\overset{(a)}{=} \int_{\Delta h_u}^{+\infty} \int_{\theta^{\frac{1}{\alpha_L}} r_{L_0}}^{+\infty} f_{R_{L_1}|R_{L_0}}(r_{L_1}|r_{L_0}) \exp\left(-2\pi\lambda_b \int_0^{l(\widetilde{d}_{L\_N}(r_{L_0}))} zp^N(z)dz\right) f_{R_{L_0}}(r_{L_0})dr_{L_1}dr_{L_0},
\end{aligned}
$$
$$(57)$$

where (a) follows from the joint PDF and null probability of inhomogenous PPP Φ_B^N, and we define $l(r) \triangleq \sqrt{r^2 - (\Delta h_u)^2}$,

$$
\widetilde{d}_{L\_N}(r_{L_0}) \triangleq \begin{cases} \Delta h_u, & \text{if} \quad \Delta h_u \leq r_{L_0} < l_{L\_N}, \\ \theta^{\frac{1}{\alpha_N}} d_{L\_N}(r_{L_0}), & \text{if} \quad r_{L_0} \geq l_{L\_N}, \end{cases}
$$
$$(58)$$

with $d_{L\_N}(r_{L_0}) \triangleq (\frac{\eta_N}{\eta_L})^{\frac{1}{\alpha_N}} r_{L_0}^{\frac{\alpha_L}{\alpha_N}}$, $l_{L\_N} \triangleq (\frac{\eta_L}{\eta_N})^{\frac{1}{\alpha_L}} (\Delta h_u)^{\frac{\alpha_N}{\alpha_L}}$. Simplifying the expression by considering the value range of r_{L_0}, we complete the proof of $\mathcal{A}_{L_0}$ in (18). Following the similar steps, we derive the probability that the typical Non-CoMP AU is associated with $\{b_{N_0}\}$ in (19).

Then, we derive the association probability when the typical AU is associated with $\{b_{L_0}, b_{L_1}\}$, which is given by

$$
\mathcal{A}_{L_0,L_1} = \Pr\left[\mathcal{B} = \{b_{L_0}, b_{L_1}\}\right] = \mathbb{E}_{R_{L_0}, R_{L_1}}\left[\Pr\left[R_{L_1} \leq \theta^{\frac{1}{\alpha_L}} R_{L_0}, R_{N_0} \geq (\frac{\eta_N}{\eta_L})^{\frac{1}{\alpha_N}} R_{L_1}^{\frac{\alpha_L}{\alpha_N}}\right]\right]. \quad (59)
$$

Following the similar steps as of the proof for $\mathcal{A}_{L_0,L_1}$, and considering the range of r_{L_0} shown in (58), we complete the proof of $\mathcal{A}_{L_0,L_1}$ in (20). Similarly, we can prove $\mathcal{A}_{N_0,N_1}$, $\mathcal{A}_{L_0,N_0}$, and $\mathcal{A}_{N_0,L_0}$, which are given by (21), (22) and (23), respectively.

C. Proof of Lemma 4

We first derive the CDF of the distance $\widetilde{R}_{L_0}$, which is given by

$$
\begin{aligned}
\Pr[R_{L_0} < r_{L_0}|\mathcal{B} = \{b_{L_0}\}] &= \frac{1}{\mathcal{A}_{L_0}}\Pr\left[R_{L_0} < r_{L_0}, \eta_L R_{L_0}^{-\alpha_L} \geq \theta\eta_N R_{N_0}^{-\alpha_N}, R_{L_0}^{-\alpha_L} \geq \theta R_{L_1}^{-\alpha_L}\right] \\
&\overset{(a)}{=} \frac{1}{\mathcal{A}_{L_0}} \int_{\Delta h_u}^{r_{L_0}} \Pr\left[R_{L_1} \geq \theta^{\frac{1}{\alpha_L}} R_{L_0}\right] \Pr\left[R_{N_0} \geq \left(\theta\frac{\eta_N}{\eta_L}\right)^{\frac{1}{\alpha_N}} R_{L_0}^{\frac{\alpha_L}{\alpha_N}}\right] f_{R_{L_0}}(r)dr \\
&\overset{(b)}{=} \frac{1}{\mathcal{A}_{L_0}}\left[\int_{\Delta h_u}^{r_{L_0}} \int_{\theta^{\frac{1}{\alpha_L}} r}^{\infty} \exp\left(-2\pi\lambda_b \int_0^{l(\widetilde{d}_{L\_N}(r))} zp^N(z)dz\right) f_{R_{L_0}, R_{L_1}}(r, r_2)dr_2 dr\right],
\end{aligned}
$$
$$(60)$$

where (a) follows from the CDF of R_{L_0}, (b) is due to the null probability of the inhomogeneous PPP $\Phi_{\mathrm{B}}^{\mathrm{N}}$, and $\widetilde{d}_{\mathrm{L\_N}}(r_{\mathrm{L}_0})$ is given by (58). At last, substituting $f_{R_{\mathrm{L}_0},R_{\mathrm{L}_1}}(r_{\mathrm{L}_0},r_{\mathrm{L}_1})$ in (15) and taking the derivative of the CDF with regards to r_{L_0}, i.e., $f_{\widetilde{R}_{\mathrm{L}_0}}(r_{\mathrm{L}_0}) = \frac{\partial F_{\widetilde{R}_{\mathrm{L}_0}}(r_{\mathrm{L}_0})}{\partial r_{\mathrm{L}_0}}$, we complete the proof of $f_{\widetilde{R}_{\mathrm{L}_0}}(r_{\mathrm{L}_0})$ in (24). Following the same steps as that of the proof for $f_{\widetilde{R}_{\mathrm{L}_0}}(r_{\mathrm{L}_0})$, we can complete the proof of $f_{\widetilde{R}_{\mathrm{N}_0}}(r_{\mathrm{N}_0})$, which is given by (25).

D. Proof of Lemma 5

To obtain the joint PDF $f_{\widetilde{R}_{\mathrm{L}_0},\widetilde{R}_{\mathrm{L}_1}}(r_{\mathrm{L}_0},r_{\mathrm{L}_1})$, we first derive the joint CDF $F_{\widetilde{R}_{\mathrm{L}_0},\widetilde{R}_{\mathrm{L}_1}}(r_{\mathrm{L}_0},r_{\mathrm{L}_1})$, which is given by

$$\Pr[R_{\mathrm{L}_0} \leq r_{\mathrm{L}_0}, R_{\mathrm{L}_1} \leq r_{\mathrm{L}_1}|\mathcal{B} = \{b_{\mathrm{L}_0}, b_{\mathrm{L}_1}\}]$$

$$= \frac{1}{\mathcal{A}_{\mathrm{L}_0,\mathrm{L}_1}}\Pr[R_{\mathrm{L}_0} \leq r_{\mathrm{L}_0}, R_{\mathrm{L}_1} \leq r_{\mathrm{L}_1}, \theta R_{\mathrm{L}_1}^{-\alpha_{\mathrm{L}}} \geq R_{\mathrm{L}_0}^{-\alpha_{\mathrm{L}}}, \eta_{\mathrm{L}} R_{\mathrm{L}_1}^{-\alpha_{\mathrm{L}}} \geq \eta_{\mathrm{N}} R_{\mathrm{N}_0}^{-\alpha_{\mathrm{N}}}]$$

$$= \frac{1}{\mathcal{A}_{\mathrm{L}_0,\mathrm{L}_1}}\int_{\Delta h_{\mathrm{u}}}^{r_{\mathrm{L}_0}}\Pr\left[R_{\mathrm{L}_1} \geq \theta^{\frac{1}{\alpha_{\mathrm{L}}}}R_{\mathrm{L}_0}\right]\Pr\left[R_{\mathrm{N}_0} \geq (\theta\frac{\eta_{\mathrm{N}}}{\eta_{\mathrm{L}}})^{\frac{1}{\alpha_{\mathrm{N}}}}R_{\mathrm{L}_1}^{\frac{\alpha_{\mathrm{L}}}{\alpha_{\mathrm{N}}}}\right]f_{R_{\mathrm{L}_0}}(r)dr$$

$$\overset{(a)}{=} \begin{cases} \frac{1}{\mathcal{A}_{\mathrm{L}_0,\mathrm{L}_1}}[\int_{\Delta h_{\mathrm{u}}}^{r_{\mathrm{L}_0}}\int_r^{r_{\mathrm{L}_1}}f_{R_{\mathrm{L}_0},R_{\mathrm{L}_1}}(r,r_2)dr_2 dr], & \text{if } r_0 \in [\Delta h_{\mathrm{u}}, l_{\mathrm{L\_N}}), \\ \frac{1}{\mathcal{A}_{\mathrm{L}_0,\mathrm{L}_1}}[\int_{l_{\mathrm{L\_N}}}^{r_{\mathrm{L}_0}}\int_r^{r_{\mathrm{L}_1}}\exp(-2\pi\lambda_b\int_0^{l\left(\theta^{\frac{1}{\alpha_{\mathrm{N}}}}d_{\mathrm{L\_N}}(r_{\mathrm{L}_0})\right)}zp^{\mathrm{N}}(z)dz)f_{R_{\mathrm{L}_0},R_{\mathrm{L}_1}}(r,r_2)dr_2 dr], & \text{if } r_0 \geq l_{\mathrm{L\_N}}, \end{cases}$$

$$(61)$$

where (a) follows from the null probability of inhomogenous PPP $\Phi_{\mathrm{B}}^{\mathrm{N}}$, At last, substituting $f_{R_{\mathrm{L}_0},R_{\mathrm{L}_1}}(r_{\mathrm{L}_0},r_{\mathrm{L}_1})$ in (15) and taking the derivative of the CDF with regards to r_{L_0} and r_{L_1}, i.e., $f_{\widetilde{R}_{\mathrm{L}_0},\widetilde{R}_{\mathrm{L}_1}}(r_{\mathrm{L}_0},r_{\mathrm{L}_1}) = \frac{\partial^2 F_{\widetilde{R}_{\mathrm{L}_0},\widetilde{R}_{\mathrm{L}_1}}(r_{\mathrm{L}_0},r_{\mathrm{L}_1})}{\partial r_{\mathrm{L}_0}\partial r_{\mathrm{L}_1}}$, we complete the proof of $f_{\widetilde{R}_{\mathrm{L}_0},\widetilde{R}_{\mathrm{L}_1}}(r_{\mathrm{L}_0},r_{\mathrm{L}_1})$ in (26). Following the same steps as that of the proof for $f_{\widetilde{R}_{\mathrm{L}_0},\widetilde{R}_{\mathrm{L}_1}}(r_{\mathrm{L}_0},r_{\mathrm{L}_1})$, we can complete the proof of $f_{\widetilde{R}_{\mathrm{N}_0},\widetilde{R}_{\mathrm{N}_1}}(r_{\mathrm{N}_0},r_{\mathrm{N}_1})$, $f_{\widetilde{R}_{\mathrm{N}_0},\widetilde{R}_{\mathrm{L}_0}}(r_{\mathrm{N}_0},r_{\mathrm{L}_0})$, and $f_{\widetilde{R}_{\mathrm{L}_0},\widetilde{R}_{\mathrm{N}_0}}(r_{\mathrm{L}_0},r_{\mathrm{N}_0})$, which are given by (27), (28) and (29), respectively. This completes the proof of Lemma 5.

E. Proof of Theorem 2

Referring to (10), the numerator $\left|\sum_{k=0}^1 (\rho_{\mathrm{u}}P_{\mathrm{t}}\zeta_v(b_k))^{\frac{1}{2}}\widetilde{\omega}_{k,0}\right|^2$ represents the square of a weighted sum of two Nakagami-m RVs. Since closed-form expression is unknown, we use the Cauchy-Schwarz's inequality to obtain the upper bound of $\left|\sum_{k=0}^1 (\rho_{\mathrm{u}}P_{\mathrm{t}}\zeta_v(b_k))^{\frac{1}{2}}\widetilde{\omega}_{k,0}\right|^2$ as follows

$$\left|\sum_{k=0}^1 (\rho_{\mathrm{u}}P_{\mathrm{t}}\zeta_v(b_k))^{\frac{1}{2}}\widetilde{\omega}_{k,0}\right|^2 = \left|\sum_{k=0}^1 (\rho_{\mathrm{u}}P_{\mathrm{t}}\zeta_v(b_k))^{\frac{1}{2}}\frac{\omega_{k0}^*}{|\omega_{k0}|}\omega_{k0}\right|^2 = \rho_{\mathrm{u}}P_{\mathrm{t}}\left(\sum_{k=0}^1 Q_k\right)^2 \leq 2\rho_{\mathrm{u}}P_{\mathrm{t}}\left(\sum_{k=0}^1 Q_k^2\right),$$

$$(62)$$

where $Q_k = (\zeta_v(b_k))^{\frac{1}{2}}\widetilde{\omega}_{k,0} = (\zeta_v(b_k))^{\frac{1}{2}}|\omega_{k,0}|$ is a scaled Nakagami-m RV. Since $\omega_{k,0} \sim$ Nakagami-m, according to the scaling property of the Gamma distribution, we have $Q_k^2 \sim \Gamma(\kappa_k = m_v, \theta_k =$

$\zeta_v(b_k)/m_v$). To achieve a tractable statistical equivalent of two Gamma RVs with different scale parameters θ_k, we adopt the method of second-order moment matching for Gamma RVs. It is shown that the equivalent Gamma distribution, denoted by $\mathcal{J} \sim \Gamma(K, \Theta)$, has the same first-order and second-order moments with the following parameters

$$K = \frac{(\sum_{k=0}^{1} \kappa_k \theta_k)^2}{\sum_{k=0}^{1} \kappa_k \theta_k^2} = \frac{m_v(\sum_{k=0}^{1} \zeta_v(b_k))^2}{\sum_{k=0}^{1}(\zeta_v(b_k))^2}, \Theta = \frac{\sum_{k=0}^{1} \kappa_k \theta_k^2}{\sum_{k=0}^{1} \kappa_k \theta_k} = \frac{\sum_{k=0}^{1} m_v(\zeta_v(b_k)/m_v)^2}{\sum_{k=0}^{1} m_v \zeta_v(b_k)}. \quad (63)$$

To derive the upper bound of the shape parameter K, we consider the following two cases: i) the two cooperative BSs are of the same type, i.e., $\mathcal{B} = \{b_{L_0}, b_{L_1}\}$ or $\mathcal{B} = \{b_{N_0}, b_{N_1}\}$; ii) the two cooperative BSs are of different types, i.e., i.e., $\mathcal{B} = \{b_{L_0}, b_{N_0}\}$ or $\mathcal{B} = \{b_{N_0}, b_{L_0}\}$. For case i), we use the Cauchy-Schwarz's inequality, which leads to $K = \frac{m_v(\sum_{k=0}^{1} \zeta_v(b_k))^2}{\sum_{k=0}^{1}(\zeta_v(b_k))^2} \leq 2m_v$, $v = L$ or N. For case ii), we derive the upper bound of K using the weighted norm inequality as $K \leq m_N + m_L$.

Given r_{L_0} and r_{L_1}, the conditional coverage probability can be derived by

$$\mathbb{P}_{L_0,L_1|r_{L_0},r_{L_1}}(T) \overset{(a)}{\leq} \text{Pr}\left[\frac{2\rho_u P_t \mathcal{J}}{\rho_t P_t \mathcal{J} + I} \geq T|r_{L_0}, r_{L_1}\right] \overset{(b)}{\approx} \text{Pr}\left[\mathcal{J} > \frac{TI}{(2\rho_u - \rho_t T)P_t}\right]$$

$$\overset{(c)}{=} \frac{\Gamma\left(K, \frac{TI}{(2\rho_u - \rho_t T) P_t \Theta}\right)}{\Gamma(K)} \overset{(d)}{=} \mathbb{E}_I\left[\sum_{k=0}^{K-1}(sI)^k \exp(-sI))\right]\bigg|_{s=\frac{T}{(2\rho_u - \rho_t T)P_t \Theta}} \quad (64)$$

$$\overset{(e)}{=} \begin{cases} \sum_{k=0}^{2m_L-1} \frac{(-s)^k}{k!} \frac{\partial^k}{\partial s^k} \widehat{\mathcal{L}}_I(s)\big|_{s=\frac{T}{(2\rho_u - \rho_t T)P_t \Theta}}, & \text{if } r_{L_0} \in [\Delta h_u, l_{L\_N}), \\ \sum_{k=0}^{2m_L-1} \frac{(-s)^k}{k!} \frac{\partial^k}{\partial s^k} \widetilde{\mathcal{L}}_I(s)\big|_{s=\frac{T}{(2\rho_u - \rho_t T)P_t \Theta}}, & \text{if } r_{L_0} \geq l_{L\_N}, \end{cases}$$

where $I \triangleq \sum_{i \in \Phi_B \setminus \{b_{L_0}, b_{L_1}\}} P_t \zeta_v(b_i)|\widetilde{\omega}_{i,0}|^2$, $\Theta = \frac{\sum_{k=0}^{1}(\zeta_L(b_{L_k}))^2}{m_L \sum_{k=0}^{1} \zeta_L(b_{L_k})}$, (a) follows from the Cauchy-Schwarz's inequality, (b) follows from the Gamma approximation by rounding the shape parameter $K = 2m_L$, and (c) is due to the fact that for a Gamma-distributed RV $Z \sim \Gamma[k_z, \theta_z]$ with integer k_z, we have $\text{Pr}[Z > x] = \frac{\Gamma(k_z, \frac{y}{\theta_z})}{\Gamma(k_z)} = \sum_{k=0}^{k_z-1} \frac{y^k \exp(-y)}{k!}$, which leads to (d). Finally, with $\frac{\partial^k}{\partial k_z}[\exp(-zY)] = (-Y)^k \exp(-zY)$, we derive (e), where the Laplace transform $\widehat{\mathcal{L}}_I(s)$ and $\widetilde{\mathcal{L}}_I(s)$ are given by (39) and (40), respectively. Finally, by averaging over r_{L_1} and r_{L_0}, we complete the proof of the coverage probability when the typical CoMP AU associating with $\mathcal{B} = \{b_{L_0}, b_{L_1}\}$ in (35) of Theorem 2. Following the same steps as that for the proof of $\mathbb{P}_{L_0,L_1}(T)$, we complete the proof of $\mathbb{P}_{N_0,N_1}(T)$, $\mathbb{P}_{L_0,N_0}(T)$, and $\mathbb{P}_{N_0,L_0}(T)$ in (36), (37), and (38), respectively. This completes the proof of Theorem 2.

References

[1] M. Vondra, M. Ozger, D. Schupke, and C. Cavdar, "Integration of Satellite and Aerial Communications for Heterogeneous Flying Vehicles," *IEEE Network*, vol. 32, no. 5, pp. 62–69, 2018.

[2] W. Saad, M. Bennis, and M. Chen, "A Vision of 6G Wireless Systems: Applications, Trends, Technologies, and Open Research Problems," *IEEE Network*, vol. 34, no. 3, pp. 134–142, 2020.

[3] A. Eldosouky, A. Ferdowsi, and W. Saad, "Drones in Distress: A Game-Theoretic Countermeasure for Protecting UAVs Against GPS Spoofing," *IEEE Internet Things J.*, vol. 7, no. 4, pp. 2840–2854, 2020.

[4] Y. Zeng, Q. Wu, and R. Zhang, "Accessing From the Sky: A Tutorial on UAV Communications for 5G and Beyond," *Proc. IEEE*, vol. 107, no. 12, pp. 2327–2375, 2019.

[5] R. Amer, W. Saad, and N. Marchetti, "Mobility in the Sky: Performance and Mobility Analysis for Cellular-Connected UAVs," *IEEE Trans. Commun.*, vol. 68, no. 5, pp. 3229–3246, 2020.

[6] X. Lin, V. Yajnanarayana, S. D. Muruganathan, S. Gao, H. Asplund, H.-L. Maattanen, M. Bergstrom, S. Euler, and Y.-P. E. Wang, "The Sky Is Not the Limit: LTE for Unmanned Aerial Vehicles," *IEEE Commun. Mag.*, vol. 56, no. 4, pp. 204–210, 2018.

[7] M. M. Azari, F. Rosas, A. Chiumento, and S. Pollin, "Coexistence of Terrestrial and Aerial Users in Cellular Networks," in *Proc. IEEE GC Wkshps*, Rio de Janeiro, Brazil, Dec. 2017, pp. 1–6.

[8] B. Van Der Bergh, A. Chiumento, and S. Pollin, "LTE in the sky: trading off propagation benefits with interference costs for aerial nodes," *IEEE Commun. Mag.*, vol. 54, no. 5, pp. 44–50, 2016.

[9] M. Karakayali, G. Foschini, and R. Valenzuela, "Network coordination for spectrally efficient communications in cellular systems," *IEEE Wirel. Commun.*, vol. 13, no. 4, pp. 56–61, 2006.

[10] T. Biermann, L. Scalia, C. Choi, W. Kellerer, and H. Karl, "How backhaul networks influence the feasibility of coordinated multipoint in cellular networks," *IEEE Commun. Mag.*, vol. 51, no. 8, pp. 168–176, 2013.

[11] M. M. Azari, G. Geraci, A. Garcia-Rodriguez, and S. Pollin, "UAV-to-UAV Communications in Cellular Networks," *IEEE Trans. Wirel. Commun.*, vol. 19, no. 9, pp. 6130–6144, 2020.

[12] M. M. Azari, F. Rosas, and S. Pollin, "Cellular Connectivity for UAVs: Network Modeling, Performance Analysis, and Design Guidelines," *IEEE Trans. Wirel. Commun.*, vol. 18, no. 7, pp. 3366–3381, 2019.

[13] H. Sun, C. Ma, L. Zhang, J. Li, X. Wang, S. Li, and T. Q. S. Quek, "Coverage Analysis for Cellular-Connected Random 3D Mobile UAVs With Directional Antennas," *IEEE Wirel. Commun. Lett.*, vol. 12, no. 3, pp. 550–554, 2023.

[14] L. Liu, S. Zhang, and R. Zhang, "CoMP in the Sky: UAV Placement and Movement Optimization for Multi-User Communications," *IEEE Trans. Commun.*, vol. 67, no. 8, pp. 5645–5658, 2019.

[15] R. Amer, W. Saad, and N. Marchetti, "Mobility in the Sky: Performance and Mobility Analysis for Cellular-Connected UAVs," *IEEE Trans. Commun.*, vol. 68, no. 5, pp. 3229–3246, 2020.

[16] Y. Tian, A. Nix, and M. Beach, "On the Performance of a Multi-Tier NOMA Strategy in Coordinated Multi-Point Networks," *IEEE Commun. Lett.*, vol. 21, no. 11, pp. 2448–2451, 2017.

[17] R. Tanbourgi, S. Singh, J. G. Andrews, and F. K. Jondral, "A Tractable Model for Noncoherent Joint-Transmission Base Station Cooperation," *IEEE Trans. Wirel. Commun.*, vol. 13, no. 9, pp. 4959–4973, 2014.

[18] M. S. Ali, E. Hossain, and D. I. Kim, "Coordinated Multipoint Transmission in Downlink Multi-Cell NOMA Systems: Models and Spectral Efficiency Performance," *IEEE Wirel. Commun.*, vol. 25, no. 2, pp. 24–31, 2018.

[19] Z. Ding, Y. Liu, J. Choi, Q. Sun, M. Elkashlan, I. Chih-Lin, and H. V. Poor, "Application of Non-Orthogonal Multiple Access in LTE and 5G Networks," *IEEE Commun. Mag.*, vol. 55, no. 2, pp. 185–191, 2017.

[20] M. S. Ali, H. Tabassum, and E. Hossain, "Dynamic User Clustering and Power Allocation for Uplink and Downlink Non-Orthogonal Multiple Access (NOMA) Systems," *IEEE Access*, vol. 4, pp. 6325–6343, 2016.

[21] A. Benjebbour, A. Li, Y. Kishiyama, H. Jiang, and T. Nakamura, "System-level performance of downlink NOMA combined with SU-MIMO for future LTE enhancements," in *Proc. IEEE GLOBECOM Wkshps*, Austin, TX, USA, Oct. 2014, pp. 706–710.

[22] W. Mei and R. Zhang, "Uplink Cooperative NOMA for Cellular-Connected UAV," *IEEE J. Sel. Topics in Signal Process.*, vol. 13, no. 3, pp. 644–656, 2019.

[23] X. Mu, Y. Liu, L. Guo, and J. Lin, "Non-Orthogonal Multiple Access for Air-to-Ground Communication," *IEEE Trans. Commun.*, vol. 68, no. 5, pp. 2934–2949, 2020.

[24] N. Senadhira, S. Durrani, X. Zhou, N. Yang, and M. Ding, "Uplink NOMA for Cellular-Connected UAV: Impact of UAV Trajectories and Altitude," *IEEE Trans. Commun.*, vol. 68, no. 8, pp. 5242–5258, 2020.

[25] T. Hou, Y. Liu, Z. Song, X. Sun, and Y. Chen, "NOMA-Enhanced Terrestrial and Aerial IoT Networks With Partial CSI," *IEEE Internet Things J.*, vol. 7, no. 4, pp. 3254–3266, 2020.

[26] S. K. Zaidi, S. F. Hasan, and X. Gui, "Outage Analysis of Ground-Aerial NOMA With Distinct Instantaneous Channel Gain Ranking," *IEEE Trans. Veh. Technol.*, vol. 68, no. 11, pp. 10 775–10 790, 2019.

[27] W. K. New, C. Y. Leow, K. Navaie, and Z. Ding, "Robust Non-Orthogonal Multiple Access for Aerial and Ground Users," *IEEE Trans. Wirel. Commun.*, vol. 19, no. 7, pp. 4793–4805, 2020.

[28] W. Mei and R. Zhang, "Cooperative NOMA for Downlink Asymmetric Interference Cancellation," *IEEE Wirel. Commun. Lett.*, vol. 9, no. 6, pp. 884–888, 2020.

[29] W. K. New, C. Y. Leow, K. Navaie, Y. Sun, and Z. Ding, "Interference-Aware NOMA for Cellular-Connected UAVs: Stochastic Geometry Analysis," *IEEE J. Sel. Areas Commun.*, vol. 39, no. 10, pp. 3067–3080, 2021.

[30] M. S. Ali, E. Hossain, and D. I. Kim, "Coordinated Multipoint Transmission in Downlink Multi-Cell NOMA Systems: Models and Spectral Efficiency Performance," *IEEE Wirel. Commun.*, vol. 25, no. 2, pp. 24–31, 2018.

[31] M. Elhattab, M. A. Arfaoui, and C. Assi, "A Joint CoMP C-NOMA for Enhanced Cellular System Performance," *IEEE Commun. Lett.*, vol. 24, no. 9, pp. 1919–1923, 2020.

[32] Z. Liu, G. Kang, L. Lei, N. Zhang, and S. Zhang, "Power Allocation for Energy Efficiency Maximization in Downlink CoMP Systems with NOMA," in *Proc. IEEE WCNC*, San Francisco, CA, USA, Mar. 2017, pp. 1–6.

[33] A. Chowdary, G. Chopra, A. Kumar, and L. R. Cenkeramaddi, "Enhanced User Grouping and Pairing Scheme for CoMP-NOMA-based Cellular Networks," in *Proc. COMSNETS*, Bangalore, India, Jan. 2022, pp. 319–323.

[34] M. Elhattab, M.-A. Arfaoui, and C. Assi, "CoMP Transmission in Downlink NOMA-Based Heterogeneous Cloud Radio Access Networks," *IEEE Trans. Commun.*, vol. 68, no. 12, pp. 7779–7794, 2020.

[35] H. Sun, X. Wang, Y. Zhang, and T. Q. S. Quek, "Performance Analysis and Cell Association Design for Drone-Assisted Heterogeneous Networks," *IEEE Trans. Veh. Technol.*, vol. 69, no. 11, pp. 13 741–13 755, 2020.

[36] J. G. Andrews, F. Baccelli, and R. K. Ganti, "A Tractable Approach to Coverage and Rate in Cellular Networks," *IEEE Trans. Commun.*, vol. 59, no. 11, pp. 3122–3134, 2011.

[37] M. Alzenad and H. Yanikomeroglu, "Coverage and Rate Analysis for Vertical Heterogeneous Networks (VHetNets)," *IEEE Trans. Wireless Commun.*, vol. 18, no. 12, pp. 5643–5657, 2019.

[38] Z. Zhang, H. Sun, and R. Q. Hu, "Downlink and Uplink Non-Orthogonal Multiple Access in a Dense Wireless Network," *IEEE J. Sel. Areas Commun.*, vol. 35, no. 12, pp. 2771–2784, 2017.